Title
Dynamic Ir(III) Photosensors for the Major Human Drug-Metabolizing Enzyme Cytochrome P450 3A4

Journal
Inorganic Chemistry, 62(7)

ISSN
0020-1669

Authors
Denison, Madeline
Ahrens, Justin J
Dunbar, Marilyn N
et al.

Publication Date
2023-02-20

DOI
10.1021/acs.inorgchem.3c00059

Peer reviewed

HHS Public Access

Author manuscript

Inorg Chem. Author manuscript; available in PMC 2024 February 20.

Published in final edited form as:

Inorg Chem. 2023 February 20; 62(7): 3305–3320. doi:10.1021/acs.inorgchem.3c00059.

Dynamic Ir(III) Photosensors for the Major Human Drug-Metabolizing Enzyme Cytochrome P450 3A4

Madeline Denison,
Department of Chemistry, Wayne State University, Detroit, Michigan 48202, United States

Justin J. Ahrens,
Department of Chemistry, Wayne State University, Detroit, Michigan 48202, United States

Marilyn N. Dunbar,
Department of Chemistry and Biochemistry, The Ohio State University, Columbus, Ohio 43210, United States

Habon Warmahaye,
Department of Chemistry and Biochemistry, The Ohio State University, Columbus, Ohio 43210, United States

Aliza Majeed,
Institute of Environmental Health Sciences, Wayne State University, Detroit, Michigan 48202, United States

Claudia Turro,
Department of Chemistry and Biochemistry, The Ohio State University, Columbus, Ohio 43210, United States

Thomas A. Kocarek,
Institute of Environmental Health Sciences, Wayne State University, Detroit, Michigan 48202, United States

Irina F. Sevrioukova,

Corresponding Authors: Claudia Turro – *Department of Chemistry and Biochemistry, The Ohio State University, Columbus, Ohio 43210, United States*; turro.1@osu.edu, **Thomas A. Kocarek** – *Institute of Environmental Health Sciences, Wayne State University, Detroit, Michigan 48202, United States*; t.kocarek@wayne.edu, **Irina F. Sevrioukova** – *Department of Molecular Biology and Biochemistry, University of California, Irvine, California 92697, United States*; sevrioui@uci.edu, **Jeremy J. Kodanko** – *Department of Chemistry, Wayne State University, Detroit, Michigan 48202, United States; Barbara Ann Karmanos Cancer Institute, Detroit, Michigan 48201, United States*; jkodanko@chem.wayne.edu.

The authors declare no competing financial interest.

ASSOCIATED CONTENT

Supporting Information

The Supporting Information is available free of charge at https://pubs.acs.org/doi/10.1021/acs.inorgchem.3c00059.

Detailed experimental procedures of synthesis of compounds **1–15** and corresponding ^{1}H NMR spectral data (including ^{13}C NMR of **1–4**); CD spectra of Δ-(L)-**6**, Λ-(D)-**6**, Δ-(D)-**6**, Λ-(L)-**6**, Δ-**12**, Λ-**12**, Δ-**13**, and Λ-**13**; electronic absorption and emission spectra of Δ,Λ-(L)-**6**, Δ,Λ-(L)-**9**, and Δ,Λ-(L)-**11**; biological assays for metal complexes (cell viability MTT assay for racemic (L)-**6**, **7**, (L)-**8**, and **12**); CYP inhibitor screening kits for racemic (L)-**6** and **12**; P450-Glo Assay for racemic (L)-**5**, (L)-**6**, **7**, (L)-**9**, and **12**; spectral binding titrations and inhibitory potency assays of all complexes **5–15** (including spectra of binding titrations of Δ-(L)-**6**, Λ-(L)-**6**, Δ-(D)-**6**, and Λ-(D)-**6**); structural studies (photophysical properties of all racemic metal complexes **5–15**); and X-ray crystallographic data for complexes Δ,Λ-(L)-**6**, Δ,Λ-(D)-**6**, Δ,Λ-**7**, Δ,Λ-(L)-**9**, Δ,Λ-**10**, Δ,Λ-**12**, Δ,Λ-(L)-**14**, Λ-(L)-**6**, Λ-**12**, and Δ-**13** bound to CYP3A4 (PDF)

Complete contact information is available at: https://pubs.acs.org/10.1021/acs.inorgchem.3c00059

Department of Molecular Biology and Biochemistry, University of California, Irvine, California 92697, United States

Jeremy J. Kodanko
Department of Chemistry, Wayne State University, Detroit, Michigan 48202, United States; Barbara Ann Karmanos Cancer Institute, Detroit, Michigan 48201, United States

Abstract

Probing the activity of cytochrome P450 3A4 (CYP3A4) is critical for monitoring the metabolism of pharmaceuticals and identifying drug–drug interactions. A library of Ir(III) probes that detect occupancy of the CYP3A4 active site were synthesized and characterized. These probes show selectivity for CYP3A4 inhibition, low cellular toxicity, K_d values as low as 9 nM, and are highly emissive with lifetimes up to 3.8 μs in cell growth media under aerobic conditions. These long emission lifetimes allow for time-resolved gating to distinguish probe from background autofluorescence from growth media and live cells. X-ray crystallographic analysis revealed structure–activity relationships and the preference or indifference of CYP3A4 toward resolved stereoisomers. Ir(III)-based probes show emission quenching upon CYP3A4 binding, then emission increases following displacement with CYP3A4 inhibitors or substrates. Importantly, the lead probes inhibit the activity of CYP3A4 at concentrations as low as 300 nM in CYP3A4-overexpressing HepG2 cells that accurately mimic human hepatic drug metabolism. Thus, the Ir(III)-based agents show promise as novel chemical tools for monitoring CYP3A4 active site occupancy in a high-throughput manner to gain insight into drug metabolism and drug–drug interactions.

Graphical Abstract

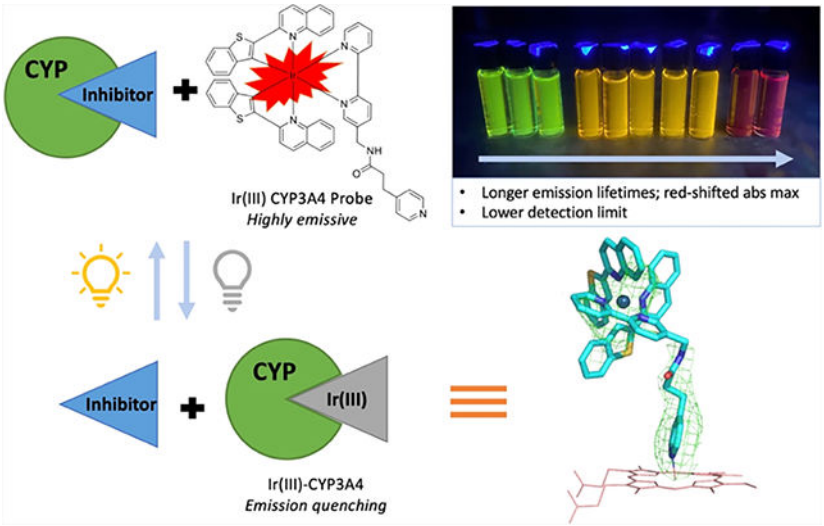

INTRODUCTION

Cytochrome P450s (CYPs) are heme-containing enzymes that are critical in biosynthesis[1–3] and metabolism of pharmaceuticals.[4,5] CYPs are generally located in the liver and in some

extrahepatic areas.[1,2,6–9] Isoform CYP3A4 is the most abundant CYP in the liver and, more importantly, is one of the major CYPs contributing to drug metabolism. CYP3A4 accounts for the metabolism of 30–50% of clinically used drugs.[8–11]

Due to the considerable fraction of drugs metabolized by CYP3A4 and its large active site, drug–drug interactions are prevalent. Unintentional inhibition of CYP3A4 can lead to increased bioavailability of the competing drug substrate and result in toxicity.[12,13] On the other hand, drug–drug interactions can be beneficial in some scenarios. An increase in drug bioavailability due to CYP3A4 inhibition can lead to productive, cost-effective treatments.[14,15] Additionally, CYP genes vary among ethnic groups causing inconsistency in pharmacokinetic responses among people.8 Induction is another challenge associated with CYPs. Rifampicin is a commonly known CYP3A4 inducer that increases CYP3A4 expression levels, thereby lowering drug bioavailability and efficacy.[16–18] Because of the multitude of pharmacokinetic interactions that involve CYP3A4, the investigation of this enzyme is crucial. Monitoring CYP3A4 active site occupancy has great potential to identify drug–drug interactions, CYP3A4 inducers, and different drug responses.

Currently, CYP activity is monitored by analyzing metabolites of marker substrates produced by CYPs at multiple time points by high-pressure liquid chromatography (HPLC), which is a time-consuming and costly process. Other methods include nonfluorescent substrates that are converted into fluorescent or luminescent products by CYP3A4; thus, emission changes are related to CYP3A4 activity.[11,19] This technique has also been utilized to successfully image CYP activity in cells.[20–23] These chemical tools are useful in probing CYP activity; however, they are irreversible and cannot measure fluctuations of activity that occur over time during drug–drug interactions or induction. More dynamic steroid-derived probes fluoresce initially and are quenched by the CYP3A4 heme upon binding.[24] While these probes are useful tools for experiments with purified CYP3A4 enzyme, they cannot be utilized for monitoring CYPs in human liver microsomes, the gold standard in drug metabolism. Organic fluorophores have short emission lifetimes, which unfortunately results in interference from autofluorescence signals derived from living cells and growth media.[25,26] Beyond CYP3A4, previous work described emissive probes acting as inhibitors for *Pseudomonas putida* $P450_{cam}$ ($P450_{cam}$).[27–30] These probes were produced by linking $P450_{cam}$ substrates to Ru(II) complexes or dansyl fluorophores, whose emission was quenched upon binding to the CYP active site due to Förster resonance energy transfer (FRET) to the heme cofactor.[27–30] Furthermore, due to its smaller active site size relative to CYP3A4, the Ru(II) complexes were not able to bind directly within the active site of $P450_{cam}$ and were instead tethered to inhibitors via linkers that spanned through the substrate access channel.[28,29]

Ir(III) complexes have emerged as robust chemical tools to sense biomolecules like amino,[25,31,32] nucleic,[31,33] and sialic acids,[34] as well as periodate.[35] They are also used to monitor biological processes such as following mitochondrial dynamics during cell death.[36–38] Moreover, cellular toxicity of Ir(III) complexes is dependent on the ligands, with many Ir(III) complexes shown to be nontoxic.[39–41] Ir(III)-based probes are advantageous due to their emissive properties and, most importantly, long phosphorescent lifetimes

ranging from hundreds of nanoseconds up to ~100 μs.[25,31,32] These long lifetimes allow for time-resolved gating, which can increase signal-to-background ratios drastically.[25]

We recently reported Ru(II)- and Ir(III)-based compounds that act as photosensors of CYP3A4 since they are quenched by the CYP3A4 active site and, upon addition of a competing CYP3A4 inhibitor or substrate, emission from the released probe is observed (Figure 1).[42] Luminescence intensity was reversely proportional to the binding affinity of the substrates and inhibitors of CYP3A4, suggesting that these probes could be useful for monitoring equilibrium binding. Importantly, CYP3A4 was found to favor Ir(III) monocationic complexes over Ru(II) dicationic probes. With this knowledge, we sought to optimize the structural, photochemical, and biological properties of Ir(III)-based probes.

Herein, we report the design, synthesis, biochemical evaluation, and application of a new series of Ir(III) CYP3A4 probes. This series was designed to include higher emission yields at longer wavelengths and longer phosphorescent lifetimes to exclude background fluorescence in biological assays. New complexes were synthesized with a number of cyclometallating ligands and side chains, including side chains with varied stereochemistry. Ten new compounds with tunable K_d values reaching the single-digit nanomolar range were co-crystallized with CYP3A4, which comprises over half of the transition-metal compounds shown by X-ray crystallographic analysis to bind to CYP3A4.[43] X-ray crystallography revealed the importance of stereochemistry and helped derive structure–activity relationships for our library of compounds, whereas functional assays revealed the probes' selectivity for CYP3A4 over other CYP isoforms. Lead compounds were shown to inhibit CYP3A4 activity in human liver hepatocarcinoma cells stably transduced with CYP3A4 (HepG2-CYP3A4), a newly developed and easily culturable cell line that provides an appropriate model for human drug metabolism, with a distinct advantage over primary human hepatocytes that are terminal and challenging to obtain. The lead Ir(III) probe was also used to demonstrate dynamic sensing of CYP3A4 active site occupancy. In contrast to existing probes, the ability to exclude background autofluorescence in cell growth media provides a new avenue for accurate probing of CYP3A4 in complex environments and simultaneously lowers the detection limits of the sensors.

RESULTS AND DISCUSSION

Compound Design and Synthesis.

We recently reported a potent Ir(III)-based CYP3A4 inhibitor that detects active site occupancy by emission assays (Figure 2).[42] This work indicated that CYP3A4 bound more strongly to monocationic Ir(III) complexes compared to related dicationic Ru(II) systems.[42] This finding led us to conserve the Ir(III) center in our new series of CYP3A4 sensors. Moreover, we found that the complex containing the large, hydrophobic ligand 2-phenylquinoline (pq) showed a higher affinity for CYP3A4 than those derived from smaller phenylpyridine (ppy) ligands. Cyclometallating ligands of similar sizes were chosen to ensure optimal interaction with hydrophobic pockets within the active site and substrate access channel, and ligands were also chosen to optimize the emission properties. This strategy led us to select pq, 2-(2,4-difluorophenyl)pyridine (dfpp), and 2-(benzo[*b*]thiophen-2-yl)quinoline (btq) as cyclometallating ligands. Our previous pq-based

compound exhibited the largest emission yield (Φ = 0.54 ± 0.06, deoxygenated CH_3CN and 0.086 ± 0.009, deoxygenated H_2O) and emission lifetime (τ = 1.6 μs, deoxygenated H_2O).[42] Ir(III) complexes containing dfpp ligands have been reported to have Φ = 0.96 ± 0.10 and long phosphorescence lifetimes, τ = 0.66 μs, in deoxygenated CH_3CN.[44] In addition, the larger extended π-electronic system of the btq ligand results in emission wavelengths that are redshifted compared to those with ligands with smaller π-systems. Reported examples of btq-based Ir(III) probes are as an oxygen sensor[45] and a perooxynitrite probe utilized *in vivo*.[46]

In our design, we sought to conserve the bipyridyl fragment of our first-generation analogues and the pyridyl tail to anchor the complex to the enzyme through direct coordination to the heme iron (type II binding). This strong mode of binding lowers the protein redox potential which can prevent the inhibitor from being oxidized by CYP3A4.[47] X-ray crystallographic analysis of our lead Ir(III) compound bound to the CYP3A4 active site showed contortion of the ligand side chain with seven atom separation between the bipyridyl group and the heme-ligating pyridine (Figure 2B). We hypothesized that Ir(III) probes could be optimized by shortening the linker length. Importantly, shortening the tether enabled the use of commercially available 3-(pyridyl)-propanoic acid analogues, including 3-(3-pyridyl)propanoic acid and 3-(4-pyridyl)propanoic acid, as well as Boc-pyridyl-alanine derivatives (3- and 4-pyridyl, L and D isomers). Points of attachment of the monodentate pyridyl group to the side chain (3- or 4-pyridyl), as well as the chirality in Boc-containing analogues, were varied to optimize hydrophobic, hydrogen-bonding, and heme binding interactions between the inhibitors and CYP3A4.

The synthesis of new Ir(III)-based inhibitors began with the preparation of bipyridyl ligands. Pyridyl acids were coupled with [2,2′-bipyridin]-5-ylmethanamine in the presence of 2-(1*H*-benzotriazol-1-yl)-1,1,3,3-tetramethyluronium hexafluorophosphate (HBTU) and *N*,*N*-diisopropylethylamine (DIPEA) to afford ligands (L)-**1**, (L)- and (D)-**2, 3**, and **4** (Scheme 1).[48] Ligands were purified by recrystallization in ethyl acetate or basic alumina column chromatography. Next, ligands **1–4** were heated with [Ir(μ-Cl)$_2$(C^N)$_2$] derivatives, where C^N = pq, dfpp, or btq (Scheme 1).[49,50] Resultant Ir(III) complexes were purified via alumina column chromatography to give complexes Δ,Λ-**5–15** (Figure 3, Table 1). The analogue Δ,Λ-(L)-**6** was carried forward to exchange the Boc group for different functional groups to further explore interactions within the CYP3A4 active site. The Boc group was first deprotected with trifluoroacetic acid (TFA) to give Δ,Λ-(L)-**6**-amine. The resultant free amine was treated with triethylamine and benzoyl chloride in dichloromethane to give Δ,Λ-(L)-**14**. The acetyl derivative Δ,Λ-(L)-**15** was synthesized in an analogous manner using two equivalents of acetic anhydride. All complexes were isolated as a mixture of Δ,Λ stereoisomers and characterized by electronic absorption, ^{1}H NMR, and electrospray ionization mass spectrometry (ESI-MS). Compounds **5–7** and **14–15** exhibit electronic absorption maxima at 435 nm, **8–10** at 360 nm, and **11–13** are significantly redshifted with a maxima at 500 nm in CH_3OH (Table 2). Electronic absorption spectra and extinction coefficients were consistent with data reported for parent complexes (Ir-(C^N)$_2$(bpy)) devoid of side chains.[44,50–52] ESI-MS data showed a peak at 1031.25 consistent with Δ,Λ-**12**. ^{1}H NMR analysis of ligand 3 reveals a singlet for the methylene unit attached to

the bipyridyl fragment at 4.41 ppm and two triplets for the ethylene unit at 3.00 and 2.62 ppm, both with coupling constants of 6.8 Hz. However, when 3 is complexed to Ir(III) metal center in Δ,Λ-**12**, these protons become diastereotopic, show complex splitting patterns, and the methylene unit is slightly shifted upfield showing a multiplet at ~4.3 ppm. The ethylene unit is also slightly shifted upfield with multiplets at ~2.8 and ~2.6 ppm. These shifts are also found in analogous complexes Δ,Λ-**7** and Δ,Λ-**10** indicating successful complexation of ligand **3** to the Ir(III) centers.

Recent synthetic methods[53–57] have emerged to resolve diastereomeric mixtures of bis-cyclometallated Ir(III) complexes as enantiopure catalysts,[58–61] chiral sensors,[62,63] lightemitting electrochemical cells (LEECs),[64] and inhibitors of tumor necrosis factor-α.[65] Stereoisomers of **6, 12**, and **13** were resolved to evaluate the role of absolute and relative stereochemistry in CYP3A4 binding.[53] Because Δ,Λ-**6** has two chiral centers, one at the metal center and one on the side chain, four unique stereoisomers are possible. The stereoisomers Δ-(L)-**6**, Δ-(D)-**6**, Λ-(L)-**6**, and Λ-(D)-**6** were produced using the chiral auxiliary (*S*)-2-(4-isopropyl-4,5-dihydrooxazol-2-yl)phenol and triethylamine following a literature method (Scheme S1).[53] Coordination of chiral auxiliaries allowed for a facile separation of Δ and Λ intermediates, which were then treated separately with TFA and corresponding ligand. Complexes were then purified by alumina column chromatography to give resolved complexes Δ-(L)-**6**, Δ-(D)-**6**, Λ-(L)-**6**, and Λ-(D)-**6**. ^{1}H NMR spectroscopic analysis confirmed the presence of single diastereomers in each sample, with specific resonances observed in the spectra of the Δ,Λ-**6** mixture now well resolved and no longer coincident with one another. Further analysis by circular dichroism spectroscopy in MeOH confirmed the following enantiomeric pairs were present: Δ-(L)-**6** and Λ-(D)-**6**; Δ-(D)-**6** and Λ-(L)-**6** (Figures S5 and S6). Likewise, enantiomeric pairs of the btq complexes Δ-**12,** Λ-**12,** Δ-**13**, and Λ-**13** were resolved using the chiral auxiliary strategy (Figure 4, Scheme S2). ^{1}H NMR spectroscopic analysis confirmed the presence of single compounds in each case and circular dichroism spectroscopy confirmed the presence of enantiomeric pairs for Δ-**12** and Λ-**12**, Δ-**13**, and Λ-**13** (Figures S7 and S8). The absolute stereochemistry of Λ-**12** and Δ-**13** was confirmed by X-ray crystallographic analysis of these compounds bound within the CYP3A4 active site (*vide infra*).

Photophysical Properties and Photochemistry.

The emission maxima, lifetimes, and quantum yields were determined to ensure complexes were suitable as luminescent CYP3A4 sensors for time-resolved gating and the results are listed in Table 2, along with absorption maxima and molar extinction coefficients. Only Λ,Δ-mixtures of L stereoisomers were examined where ligand stereochemistry is indicated.

The emission lifetimes of all complexes were relatively long, $\tau > 1\ \mu s$, where the longest lifetime was recorded for Δ,Λ-**12** with $\tau = 7.6\ \mu s$ in deaerated methanol (Table 2). The observed lifetimes and quantum yields were similar to those reported for other bis-cyclometallated Ir(III) complexes.[46,52,66–68] Quenching of emission was evident in the presence of oxygen likely due to energy transfer to generate $^1O_2$, as previously reported for related Ir(III) complexes.[69,70] Importantly, the lifetimes of the Ir(III) complexes in air are longer than those of common organic probes, which typically exhibit lifetimes in

the low nanosecond range. The lifetimes of complexes Δ,Λ-**7** and Δ,Λ-**12** were further examined in water and at 37 °C in cell media used to culture HepG2-CYP3A4 cells (Table 3). Significantly, Δ,Λ-**12** displayed an emission lifetime of 3.8 μs in cell media. Such long lifetimes are advantageous and allow for exclusion of background fluorescence of biomolecules and fluorogenic substrates found in assays.

Consistent with our previous results,[42] pq-containing complexes **5–7, 14**, and **15** were the most emissive overall, with emission quantum yields as high as 0.18(2) in deaerated H_2O (Table 2). Similar $\mathbf{\Phi}_{em}$ values were measured for the dfpp-based complexes, **8–10**, whereas those containing btq cyclometallating ligands, **11** and **12**, exhibit lower quantum yields. High luminescence intensity is favorable to not only provide an emissive switch but also to lower detection limits in assays so that less compound is needed to monitor CYP3A4, thus lowering the probability that the probe will perturb complex cellular systems. Although the btq complexes had the longest emission lifetimes, the respective quantum yields were 2-fold lower than for the majority of the library. Importantly, these quantum yields were consistent with reported values, with btq compounds showing enough emission to be useful as chemical tools to observe *in vivo*.[46,52]

Biological Studies.

All complexes were evaluated to determine CYP3A4 binding and inhibitory properties. IC_{50} values were determined using full-length recombinant CYP3A4, cytochrome P450 reductase, and 7-benzyloxy4-(trifluoromethyl)coumarin (BFC) as a substrate. Inhibition was evaluated by monitoring BFC *O*-debenzylase activity of CYP3A4 and the formation of a fluorescent product. The remaining activity was calculated relative to DMSO-containing control (100% activity) and plotted *vs* inhibitor concentration. The IC_{50} values were derived from fittings to the response curves. Spectral dissociation constants (K_d) were determined based on equilibrium titrations of Δ3–22 truncated CYP3A4 with small aliquots of inhibitors. The K_d values were derived from fittings to the plots of the ligand-induced absorbance change vs ligand concentration. Both the IC_{50} and K_d values were in the nanomolar range with no strong correlation (Table 4). The IC_{50} data indicate that the larger pq-containing complexes were more potent inhibitors than the smaller dfpp analogues, which is consistent with our previous observations on pq *vs* 2-phenylpyridine (ppy) analogues.[42] The btq-containing complexes followed the trend and, on average, were more potent than the dfpp probes. Moreover, spectral measurements revealed that all compounds except (L)-**5** and (L)-**8** induce classic type II spectral changes in CYP3A4, with a characteristic redshift in the Soret band and perturbations in the Q-band region. As mentioned previously, this strong binding mode is preferable, as it prevents metabolic oxidation of CYP3A4 inhibitors. In contrast, compounds (L)-**5** and (L)-**8** perturb the Soret but not Q-bands. This could be due to steric constraints because the heme-ligating N-pyridine is in *meta*-position but *para* in all other compounds. Nonetheless, (L)-**5** and (L)-**8** exhibit comparable IC_{50} values for CYP3A4. In accordance with our previous findings,[43] this suggests that hydrophobic and aromatic interactions mediated by the Ir(III) complexes rather than their heme-ligating ability primarily define the binding and inhibitory strength.

Interestingly, equilibrium binding and inhibitory assays did not reveal a strong preference of CYP3A4 for specific stereoisomers of **6, 12**, and **13**. For complexes **6** and **13**, the IC_{50} values were within the narrow range (120–143 and 168–173 nM, respectively; Table 4), meaning that chirality at the metal center does not strongly influence the propensity to inhibit CYP3A4. For Δ-**12** and Λ-**12**, the IC_{50} was also similar (235 and 255 nM, respectively) but substantially lower for Δ,Λ-**12** (177 nM). Why the racemic mixture is more potent is unclear at the moment. For all groups except **13**, the spread in K_d was much larger: from 2- to 3-fold (Table 4). Interestingly, the K_d values for racemic (L)-**6** and (D)-**6** resembled those for respective Λ-(L)-**6** and Δ-(D)-**6** stereoisomers, but for racemic **12** the K_d was roughly an average. This was an indication that some conformers could be preferably selected by CYP3A4, at least during lengthy equilibrium titrations. Short preincubation of CYP3A4 with probes during inhibitory assays (2 *vs* 15–20 min for spectral titrations) may be insufficient for conformer recognition. The lack of strong preference for stereoisomers could also be explained by an extreme conformational flexibility of CYP3A4 and its large, expandable active site that can accommodate a large variety of compounds, sometimes two or more at the same time.

To better understand structure–activity relationships and get insights into the probe binding modes, we co-crystalized CYP3A4 with 10 compounds from this series and determined the X-ray structures of the inhibitory complexes to 2.05–2.30 Å resolution (Tables S1–S4). Structural comparison allowed us to pinpoint differences and common trends. The common feature of the racemic compounds, (L)-**6**, (D)-**6**, **7**, (L)-**9, 10, 12**, and (L)-**14**, was a poorly defined electron density for the metal complex, possibly due to its multiple orientations (Figure 5A–G). During structural refinement, both stereoisomers were used for fitting but for all compounds except **10**, the Λ conformer provided the best fit. This was another indication that CYP3A4 may distinguish and preferably bind one stereoisomer over another. As expected, the Ir(III) fragment was more ordered when the individual stereoisomers were bound to CYP3A4, as evident from a better quality of electron density maps (Figure 5H–J), with **Δ-12** being the best defined ligand.

Unlike the Ir(III) center, electron density for the heme-ligating pyridine was well seen in all structures, allowing unambiguous fitting. As seen from a structural overlay (Figure 5K), the pyridine tilt angle varied insignificantly (by <7°), whereas the Fe–N distance was within the 1.87–2.05 Å range for all probes except Δ,Λ-(L)-**14**, which established the longest heme coordinating bond (2.20 Å). Even so, Δ,Λ-(L)-**14** was a more potent inhibitor than Δ,Λ-(L)-**9**, one of the probes with the shortest Fe–N distance (1.88 Å). Another outlier was Δ,Λ-**10**, which formed a short Fe–N bond (1.89 Å) but had the highest K_d in the series (356 nM). The latter phenomenon might be explained by the ability of **10** to bind to CYP3A4 in an alternative orientation, where the terminal pyridine orients parallel to the heme, leading to the Fe–N bond dissociation (Figure S10). The fact that **10** was a potent inhibitor (IC_{50} of 140 nM), and the general lack of correlation between the titration and inhibitory data imply once again that the heme ligation does not significantly affect the inhibitory strength. Thus, the spectral K_d, reflecting changes in heme coordination, cannot serve for prediction of the inhibitory potency of Ir(III) compounds.

The fragment linking the terminal pyridine to the metal cage is poorly defined in racemic inhibitors but becomes more ordered upon attachment of the NHBoc side group, with Δ,Λ-(L)-6 and Δ,Λ-7 being the exceptions (Figure 5B,C). The side-group moiety stabilizes the ligand binding mode by promoting hydrophobic and, for some compounds, polar interactions with the active site Ser119. However, these interactions do not notably improve K_d and IC_{50}, although compounds capable of H-bonding to Ser119, Λ-(L)-6, Δ,Λ-(L)-6 and Δ,Λ-(L)-9, tend to be tight binders.

To sum up, spectral, functional, and structural data suggest that the inhibitory potency of the Ir(III) probes is primarily defined by the chemical nature of the metal complex, while contribution of the side-group and heme-ligating functionalities is less important. As a result, spectral K_d cannot serve as a reliable parameter for IC_{50} prediction. CYP3A4 might distinguish between stereoisomers during prolonged equilibrium titrations and was found to preferably select Λ-conformers during crystallization. However, the impact of stereochemistry on IC_{50} is negligible, if any.

The apparent indifference of CYP3A4 toward specific inhibition by Δ *vs* Λ stereoisomers is likely related to its large and expandable active site. Indeed, CYP3A4 is promiscuous enzyme that metabolizes a wide range of endogenous substrates and drugs, therefore, the lack of a strong preference for specific stereoisomers can easily be explained. Importantly, the ability of CYP3A4 to accommodate larger molecules *vs* other CYP isoforms can be harnessed to create specific probes for this major human drug-metabolizing enzyme (*vide infra*). Prior research has shown specificity of Δ or Λ stereoisomers for binding to biomolecules, such as DNA and proteins. For example, both Δ and Λ isomers of tris(4,7-diphenyl-1,10- phenanthroline)ruthenium(II) bind to left-handed Z-DNA; however, only the Δ isomer binds to righthanded B-DNA.[71] Enantioselective cleavage of DNA occurs with cis-$[Rh(phen)_2(phi)^{3+}]$ (phi = 9,10-phenanthrenequinone diimine) where the Δ enantiomer is able to efficiently intercalate the 5′-pyr-pyr-pur-3′ steps and photocleave DNA.[72] Additionally, a half-sandwiched Ru(II) complex has been reported as a “selectivity switch” where Δ isomers are selective for kinases GSK3 and Pim-1 and Λ isomers are selective for PAK1.[73] On the other hand, polypyridyl Ir(III) complexes designed to inhibit carbonic anhydrase, histone deacetylases, and trypsin and only trypsin showed chiral preference of Δ isomer.[74]

To evaluate the ability of our probes to select CYP3A4 over CYP isoforms, we determined the IC_{50} values for Δ,Λ-(L)-**6** and Δ,Λ-**12** against CYP3A4, CYP2C9, and CYP1A2 using commercially available inhibitor screening kits (BioVision). Unlike experiments described in Table 4, these kit experiments that were carried out with Δ3–22 CYP3A4, these kit experiments utilize microsomal recombinant CYPs, an NADPH generating system, and resorufin substrates that fluoresce upon CYP oxidation. Because these are different experimental conditions, data from these kits cannot be compared directly with data in Table 4. CYP activity was determined by relative inhibition of product fluorescence to control and IC_{50} values were calculated based on percent activity *vs* log(molarity) dose–response plots. The compound Δ,Λ-(L)-**6** had a >100-fold selectivity for CYP3A4 with IC_{50} values of >100 μM for both CYP1A2 and CYP2C9 *vs* 0.91 ± 0.07 μM for CYP3A4. The racemic probe Δ,Λ-**12** containing the btq ligand showed IC_{50} values of 72 ± 5, 17 ± 4, and 2.3 ± 0.4 μM for

CYP1A2, CYP2C9, and CYP3A4, respectively, indicating Δ,Λ-**12** was >7-fold selective for CYP3A4 *vs* other isoforms (Table 5).

The ability of complexes to inhibit cellular CYP3A4 was assessed in human hepatocarcinoma HepG2 cells stably transduced with a lentiviral vector expressing CYP3A4. HepG2 cells have low to no expression of most drug-metabolizing CYPs, but when they are engineered to stably express CYPs, protein levels reach those in primary human hepatocytes.[75–79] Thus, the HepG2-CYP3A4 cell line is a convenient *in vitro* model for mimicking drug metabolism in the human liver. Because the chirality at the metal center did not strongly influence the inhibitory potency of the Ir(III)-based probes, studies were carried out with stereoisomeric mixtures of five compounds Δ,Λ-(L)-**5**, Δ,Λ-(L)-**6**, Δ,Λ-**7**, Δ,Λ-(L)-**9**, and Δ,Λ-**12**. To determine the CYP3A4 inhibitory activity of these probes, HepG2-CYP3A4 cells were used in conjuction with a bioluminescent P450-Glo CYP3A4 assay that utilizes a CYP3A4-specific substrate, luciferin-IPA. HepG2-CYP3A4 cells were treated with vehicle (0.1% DMSO), Ir(III) compounds (1–10 or 0.1–10 μM), or CYP3A4 inhibitors (1 μM ketoconazole or 0.1–1 μM ritonavir) as a positive control for 3 h before addition of substrate. After 1 h incubation, aliquots were taken from triplicate wells to measure luminescence. Notably, a strong dose-dependent decrease in luminescence was observed (Figure 6). Importantly, the data presented in Figure 6 indicate that Ir(III)-based probes can penetrate HepG2-CYP3A4 cells and inhibit CYP3A4 in the nanomolar to low micromolar range.

Next, to determine the ability of our compounds to function as probes in HepG2-CYP3A4 cells, cellular viability assays were conducted with compounds Δ,Λ-(L)-**5**, Δ,Λ-(L)-**6**, Δ,Λ-**7**, Δ,Λ-(L)-**9**, and Δ,Λ-**12**. The cells were seeded in 96-well plates (7000 cells/well) and incubated for 18 h before treatment with compounds (100 nM to 50 μM) or vehicle control. After 72 h of treatment, cell viability was determined using the 3-(4,5-dimethylthiazol-2-yl)-2,5-diphenyl tetrazolium bromide (MTT) assay. Interestingly, the dfpp complex Δ,Λ-(L)-**9** was found to be nontoxic with an EC_{50} value >50 μM, whereas Δ,Λ-(L)-**6**, Δ,Λ-**7**, and Δ,Λ-**12** showed EC_{50} values ranging from 16 to 21 μM (Table 6). Although these probes are potentially harmful to cells at higher concentrations, cellular toxicity can be avoided or largely minimized when Ir(III) complexes are used as photosensors at low concentrations, specifically in the nanomolar range.

To ensure our Ir(III) complexes would behave as suitable probes, we sought to take advantage of the long lifetimes of Ir(III) and determine the detection limits in media and cells in microplate assays. Lower detection limits were preferred to reduce the concentration of Ir(III) needed to achieve desired results of emission turn-on with minimal disturbance of the system and toxicity. We intially tested the detection limits of lead probe Δ,Λ-(L)-**6** due to its high luminescence intensity, long emission lifetime, relative potency, and selectivity. When Δ,Λ-(L)-**6** was excited at 400 nm in media (λ_{em} = 560 nm), we found that the difference in emission from media was statistically significant at concentrations above 500 nM (statistical significance $p < 0.05$; $p = 0.05$ for 300 nM; $p = 0.01$ for 500 nM). However, when a lag time of 15 μs was applied in the acquisition of emission, statistical significance was achieved at concentrations as low as 100 nM (Figure 7A). This 5-fold decrease in detection limit highlights the power of time-resolved gating. We also predicted

that excitation at longer wavelengths would further reduce fluorescence contributions from the media, leading us to test detection limits of Δ,Λ-**12**. Excitation of Δ,Λ-**12** at 500 nm (λ_{em} = 700 nm) in media showed strong statistical significance at 100 nM where emission increased about 3-fold from media. A lag time of 15 μs improved this detection limit and conveyed a 6-fold increase in emission from media to 100 nM (Figure 7B). It is important to note that emission intensity between Δ,Λ-**12** and Δ,Λ-(L)-**6** cannot be directly compared since Δ,Λ-**12** has lower emission yields (*vide supra*) and background fluorescence is omitted more efficiently and results in an overall lower emission intensity. These results substantiated the value of time-resolved gating in conjunction with longer excitation wavelengths to drastically decrease detection limits. Finally, detection limits were evaluated in a microplate assay using live HepG2-CYP3A4 cells. Cells were treated with Δ,Λ-**12** and after 4 h incubation, emission was monitored with a 15 μs lag time. As shown in Figure 7C, statistical significance (p = 0.000197) was achieved at 100 nM. Thus, Δ,Λ-**12** was chosen as our Ir(III) probe for further investigation.

Two potent CYP3A4 inhibitors, ketoconazole (KCZ; K_d of 25 nM; our data) and ritonavir (RIT; K_d = 19 nM)[82] were chosen as test inhibitors and midazolam as a test substrate (MDZ, K_d of 5 μM)[80] to evaluate whether Δ,Λ-**12** can be used for dynamic assessment of the occupancy of the CYP3A4 active site. The binding affinity of Δ,Λ-12 is comparable to or much higher than for the test compounds (K_d of 24 nM, Table 4), and thus it could compete for the active site. To demonstrate the competitive binding to CYP3A4, we followed emission changes in the presence of the probe and test compounds, added in a different order. Only Δ,Λ-**12** emits upon excitation at 500 nm. When Δ,Λ-**12** was mixed with substoichiometric CYP3A4, up to 60–70% of probe's emission was quickly quenched as a result of the inhibitory complex formation (Figure 8A). However, the emission yield was almost fully recovered (up to ~85%) upon addition of equimolar KCZ (up to ~85%), meaning that KCZ easily displaces the probe from the CYP3A4 active site. In a separate experiment, the order of addition was reversed and Δ,Λ-**12** was mixed with nonemitting KCZ-bound CYP3A4. As expected, addition of the probe led to a spike in emission, which was decreased by ~15% after 5 min incubation (Figure 8B). This could reflect two consecutive events: displacement of bound KCZ by Δ,Λ-12, followed by quenching of the bound probe by the heme. Emission changes in the presence of RIT were similar and not shown. Unlike KCZ and RIT, MDZ does not ligate to heme and, hence, binds much weaker to CYP3A4. As a result, MDZ cannot displace the CYP3A4-bound Δ,Λ-(L)-12 as effectively as KCZ, with ~30% fluorescence recovered after 5 min incubation (Figure 8C). Likewise, the fluorescence spike caused by the addition of Δ,Λ-**12** to MDZ-bound CYP3A4 was decreased by 30% in 5 min (Figure 8D). These results demonstrate that Δ,Λ-**12** and, possibly, other Ir(III) probes can compete with and displace CYP3A4 ligands to the extent proportional to their binding affinity.

To confirm that emission changes correspond to changes in the CYP3A4 active site occupancy, absorbance spectroscopy was utilized to monitor ligand-dependent changes in the Soret band. Oxidized CYPs absorb at 415–418 nm and spectral shifts occur when a substrate or inhibitor enters the active site and alters the heme coordination state.[11,81] MDZ and many other substrates displace the distal water molecule, leading to a high-spin shift

with the concomitant 385–395 nm peak formation (type I spectral change). KCZ, RIT, and other inhibitors that ligate to the heme cause a low-spin transition, accompanied by the Soret peak shift to 420–424 nm and perturbations in the Q-bands (type II spectral change).[11,81] For consistency with the fluorescence measurements, spectral measurements on CYP3A4 were done with Δ,Λ-**12** added either before or after the test compound. CYP3A4 has the Soret peak at 420 nm when bound to Δ,Λ-**12** and at 422 nm for the KCZ- and RIT-bound forms, which allowed us to detect displacement of one inhibitor by another. In accordance with the fluorescence measurements (Figure 8A,B), Δ,Λ-**12** had only a limited ability to displace KCZ, but KCZ could easily displace Δ,Λ-**12**, as evident from a partial, 422 to 421 nm, and full Soret shifts, 420 to 422 nm, respectively (Figure 9A,B). Spectral changes for RIT were virtually identical and are not shown. In contrast, Δ,Λ-**12** could more effectively compete with MDZ. The addition of Δ,Λ-12 to MDZ-bound CYP3A4 led to a drastic spectral change due to a high-to-low-spin transition, meaning that the majority of MDZ dissociated and Δ,Λ-12 ligated to the heme (Figure 9D). Likewise, when MDZ was added to Δ,Λ-12-bound CYP3A4, only a residual high-spin shift was observed, indicating the limited capacity of MDZ to compete with the probe (Figure 9C). Thus, spectral experiments confirmed the ability of Δ,Λ-**12** to compete for the binding to the CYP3A4 active site in a ligand-dependent manner.

Beyond the ability of our Ir(III) sensors to monitor active site occupancy, it is important to note that these probes are metal-based enzyme inhibitors, which are far less common than their organic counterparts. Indeed, there are only a few metal-based enzyme inhibitors that are Ir(III)-based.[82–84] Furthermore, the probes described in this manuscript are among a small handful of Ir(III) complexes ever characterized to bind within protein active sites.[85–92]

Because our Ir(III) probes are well tolerated in HepG2-CYP3A4 cells, future investigations will be directed toward monitoring active site occupancy in live cells. HepG2-CYP3A4 cells model human drug metabolism better than purified enzymes and human liver microsomes, which cannot recapitulate the complex cellular environment and complete physiology of human hepatocytes. The HepG2-CYP3A4 cell line is easy to culture and has CYP3A4 levels as high as those in human liver microsomes.[75,76] Also, because the whole cellular system is intact, emission assays in cells would reveal if a drug is unable to penetrate the cell membrane or enters a different cellular compartment. Simple emission assays in cells have the potential to reveal how long it takes for the drug to penetrate the cell and undergo metabolism. Emission assays can be developed further to determine if a drug is acting as a CYP3A4 inducer and whether drug–drug interactions take place.

Due to the bright emission of Ir(III) complexes, there are several reports of these probes used in live cell imaging, including the detection of hypoxia,[45,93–95] hypochlorite,[52] cysteine,[96–98] and peroxynitrite.[46] Ir(III) species have also been designed strategically to react with fluorescent substrates (via the click reaction[84] or cyclization[99]) to increase their emission and lifetime. These long luminescence lifetimes allow for proper distinguishing from the short-lived autofluorescence found in cell media. Furthermore, reported Ir(III) probes have also been utilized *in vivo*.[37,46] Because CYP3A4 metabolism of anticancer drugs can lead to CYP3A4 overexpression and *in situ* metabolism in tumor sites,[100–103] *in vivo* imaging using Ir(III) CYP3A4 photosensors has the potential to monitor if and when

drug uptake and metabolism is occurring in extrahepatic areas. Thus, our Ir(III) probes have many potential future applications in drug metabolism studies, where they could inform researchers on the duration of metabolism by CYP3A4, induction, drug–drug interactions, and *in situ* metabolism *in vivo*.

CONCLUSIONS

In conclusion, we report a library of Ir(III)-based probes for CYP3A4. X-ray crystallographic analysis of these compounds bound within the CYP3A4 active site revealed structure–activity relationships among our library. Stereoisomers of compounds **6**, **12**, and **13** were resolved to elucidate whether CYP3A4 has preference for specific stereoisomers. All compounds are brightly emissive and have long emission lifetimes. Surprisingly, Δ,Λ-**12** was the optimal probe for our assays despite having a relatively small emission quantum yield due to a much longer excitation wavelength and emission lifetime which allowed for lifetime gating. The longer excitation wavelength and use of time-resolved gating lowered detection limits, thereby avoiding cellular toxicity and inhibition of other CYP isoforms. While use of fluorogenic CYP3A4-specific substrates clearly depicts CYP3A4 activity, disadvantages include these assays are generally conducted in an isolated system containing purified CYP3A4 enzyme and do not depict activity fluctuations. On the other hand, our Ir(III)-based probes are well tolerated in HepG2-CYP3A4 cells and Δ,Λ-**12** could displace or be displaced from the CYP3A4 active site by competing inhibitors or substrates. Collectively, our data demonstrate that the Ir(III)-based probes could serve as novel chemical tools for efficient and low-cost monitoring of CYP3A4 activity and active site occupancy by simple emission measurements. While our Ir(III)-based probes provide many advantages, changes in luminescence could be a result of nonspecific binding in a cellular system. Future work will be dedicated toward applying these probes in complex systems, such as HepG2-CYP3A4 cells, and carrying out control experiments in HepG2-empty vector cells to elucidate if emission changes are specifically related to CYP3A4 allowing for eventual monitoring of time-dependent drug metabolism, CYP3A4 induction and drug–drug interactions.

Supplementary Material

Refer to Web version on PubMed Central for supplementary material.

ACKNOWLEDGMENTS

The authors gratefully acknowledge the National Science Foundation (CHE 2102508, CHE 1764235), the National Institutes of Health (ES025767 and T32GM142519), Richard Barber Interdisciplinary Research Program, and Wayne State University for support of this research. NMR resources are supported by the National Institutes of Health (S10OD028488), and High Resolution Mass Spectrometry Resources are supported by R01 GM098285–07S1. The authors thank Dr. Lei Guo of the National Center for Toxicology Research for generously providing HepG2-CYP3A4 cells. They also thank Timothy Stemmler for help with acquiring CD spectra. This work involves research carried out at the Stanford Synchrotron Radiation Lightsource (SSRL) beamline 12–2 and the Advanced Light Source beamline 5.0.2. Use of the Stanford Synchrotron Radiation Lightsource, SLAC National Accelerator Laboratory, is supported by the U.S. Department of Energy, Office of Science, Office of Basic Energy Sciences under Contract No. DE-AC02–76SF00515. The SSRL Structural Molecular Biology Program is supported by the DOE Office of Biological and Environmental Research, and by the National Institutes of Health, National Institute of General Medical Sciences (P30GM133894). Beamline 5.0.2 of the Advanced Light Source, a U.S. DOE Office of Science User Facility under Contract No. DE-AC02–05CH11231, is supported in part by the ALS-ENABLE program funded by the National Institutes of Health, National Institute of General Medical Sciences, grant P30

GM124169–01, and NIEHS Center grant (National Institutes of Health, National Institute of Environmental Health Sciences P30ES020957).

REFERENCES

(1). Lynch T; Price A The Effect of Cytochrome P450 Metabolism on Drug Response, Interactions, and Adverse Effects. Am. Fam. Physician 2007, 76, 391–396. [PubMed: 17708140]

(2). Seliskar M; Rozman D Mammalian Cytochromes P450—Importance of Tissue Specificity. Biochim. Biophys. Acta, Gen. Subj. 2007, 1770, 458–466.

(3). McDonnell AM; Dang CH Basic Review of the Cytochrome P450 System. J. Adv. Pract. Oncol. 2013, 4, No. 263. [PubMed: 25032007]

(4). Isin EM; Guengerich FP Complex Reactions Catalyzed by Cytochrome P450 Enzymes. Biochim. Biophys. Acta, Gen. Subj. 2007, 1770, 314–329.

(5). Li AP; Kaminski DL; Rasmussen A Substrates of human hepatic cytochrome P450 3A4. Toxicology 1995, 1–8.

(6). de Wildt SN; Kearns GL; Leeder JS; van den Anker JN Cytochrome P450 3A: Ontogeny and Drug Disposition. Clin. Pharmacokinet. 1999, 37, 485–505. [PubMed: 10628899]

(7). Lin JH; Lu AYH Inhibition and Induction of Cytochrome P450 and the Clinical Implications: Clin. Pharmacokinet. 1998, 35, 361–390.

(8). Zanger UM; Schwab M Cytochrome P450 Enzymes in Drug Metabolism: Regulation of Gene Expression, Enzyme Activities, and Impact of Genetic Variation. Pharmacol. Ther. 2013, 138, 103–141. [PubMed: 23333322]

(9). Lolodi O; Wang Y-M; Wright WC; Chen T Differential Regulation of CYP3A4 and CYP3A5 and Its Implication in Drug Discovery. Curr. Drug Metab. 2018, 18, 1095–1105.

(10). Guengerich FP CYTOCHROME P-450 3A4: Regulation and Role in Drug Metabolism. Annu. Rev. Pharmacol. Toxicol. 1999, 39, 1–17. [PubMed: 10331074]

(11). Sevrioukova IF; Poulos TL Current Approaches for Investigating and Predicting Cytochrome P450 3A4-Ligand Interactions. In Monooxygenase, Peroxidase and Peroxygenase Properties and Mechanisms of Cytochrome P450; Hrycay EG., Bandiera SM., Eds.; Advances in Experimental Medicine and Biology; Springer International Publishing: Cham, 2015; Vol. 851, pp 83–105.

(12). Bailey DG; Malcolm J; Arnold O; Spence JD Grapefruit Juice–Drug Interactions. Br. J. Clin. Pharmacol. 1998, 46, 101–110. [PubMed: 9723817]

(13). Dresser GK; Spence JD; Bailey DG Pharmacokinetic-Pharmacodynamic Consequences and Clinical Relevance of Cytochrome P450 3A4 Inhibition. Clin. Pharmacokinet. 2000, 38, 41–57. [PubMed: 10668858]

(14). Chapman SA; Lake KD Considerations for Using Ketoconazole in Solid Organ Transplant Recipients Receiving Cyclosporine Immunosuppression. J. Transpl. Coord. 1996, 6, 7.

(15). Brayer SW; Reddy KR Ritonavir-Boosted Protease Inhibitor Based Therapy: A New Strategy in Chronic Hepatitis C Therapy. Expert Rev. Gastroenterol. Hepatol. 2015, 9, 547–558. [PubMed: 25846301]

(16). Back DJ; Breckenridge AM; Crawford F; MacIver M; Orme M; Park BK; Rowe PH; Smith E The Effect of Rifampicin on Norethisterone Pharmacokinetics. Eur. J. Clin. Pharmacol. 1979, 15, 193–197. [PubMed: 37091]

(17). Bolt HM; Kappus H; Bolt M Effect of Rifampicin.Treatment on the Metabolism of Oestradiol and 17α-Ethinyloestradiol by Human Liver Microsomes. Eur. J. Clin. Pharmacol. 1975, 8, 301–307. [PubMed: 1233229]

(18). Yamashita F; Sasa Y; Yoshida S; Hisaka A; Asai Y; Kitano H; Hashida M; Suzuki H Modeling of Rifampicin-Induced CYP3A4 Activation Dynamics for the Prediction of Clinical Drug-Drug Interactions from In Vitro Data. PLoS One 2013, 8, No. e70330. [PubMed: 24086247]

(19). Raunio H; Pentikäinen O; Juvonen RO Coumarin-Based Profluorescent and Fluorescent Substrates for Determining Xenobiotic-Metabolizing Enzyme Activities In Vitro. Int. J. Mol. Sci. 2020, 21, 4708. [PubMed: 32630278]

(20). Ning J; Liu T; Dong P; Wang W; Ge G; Wang B; Yu Z; Shi L; Tian X; Huo X; Feng L; Wang C; Sun C; Cui J; James TD; Ma X Molecular Design Strategy to Construct the Near-Infrared

Fluorescent Probe for Selectively Sensing Human Cytochrome P450 2J2. J. Am. Chem. Soc. 2019, 141, 1126–1134. [PubMed: 30525564]

(21). Dai Z-R; Ge G-B; Feng L; Ning J; Hu L-H; Jin Q; Wang D-D; Lv X; Dou T-Y; Cui J-N; Yang L A Highly Selective Ratiometric Two-Photon Fluorescent Probe for Human Cytochrome P450 1A. J. Am. Chem. Soc. 2015, 137, 14488–14495. [PubMed: 26488456]

(22). Ning J; Tian Z; Wang B; Ge G; An Y; Hou J; Wang C; Zhao X; Li Y; Tian X; Yu Z; Huo X; Sun C; Feng L; Cui J; Ma X A Highly Sensitive and Selective Two-Photon Fluorescent Probe for Real-Time Sensing of Cytochrome P450 1A1 in Living Systems. Mater. Chem. Front. 2018, 2, 2013–2020.

(23). Dai Z-R; Feng L; Jin Q; Cheng H; Li Y; Ning J; Yu Y; Ge G-B; Cui J-N; Yang L A Practical Strategy to Design and Develop an Isoform-Specific Fluorescent Probe for a Target Enzyme: CYP1A1 as a Case Study. Chem. Sci. 2017, 8, 2795–2803. [PubMed: 28553516]

(24). Chougnet A; Grinkova Y; Ricard D; Sligar S; Woggon W-D Fluorescent Probes for Rapid Screening of Potential Drug–Drug Interactions at the CYP3A4 Level. ChemMedChem 2007, 2, 717–724. [PubMed: 17357170]

(25). Huang K; Bulik IW; Martí AA Time-Resolved Photoluminescence Spectroscopy for the Detection of Cysteine and Other Thiol Containing Amino Acids in Complex Strongly Autofluorescent Media. Chem. Commun. 2012, 48, 11760.

(26). Zhao Q; Huang C; Li F Phosphorescent Heavy-Metal Complexes for Bioimaging. Chem. Soc. Rev. 2011, 40, 2508. [PubMed: 21253643]

(27). Dunn AR; Dmochowski IJ; Bilwes AM; Gray HB; Crane BR Probing the Open State of Cytochrome P450cam with Ruthenium-Linker Substrates. Proc. Natl. Acad. Sci. U.S.A. 2001, 98, 12420–12425. [PubMed: 11606730]

(28). Dmochowski IJ; Crane BR; Wilker JJ; Winkler JR; Gray HB Optical Detection of Cytochrome P450 by Sensitizer-Linked Substrates. Proc. Natl. Acad. Sci. U.S.A. 1999, 96, 12987–12990. [PubMed: 10557259]

(29). Hays A-MA; Dunn AR; Chiu R; Gray HB; Stout CD; Goodin DB Conformational States of Cytochrome P450cam Revealed by Trapping of Synthetic Molecular Wires. J. Mol. Biol. 2004, 344, 455–469. [PubMed: 15522298]

(30). Dunn AR; Hays A-MA; Goodin DB; Stout CD; Chiu R; Winkler JR; Gray HB Fluorescent Probes for Cytochrome P450 Structural Characterization and Inhibitor Screening. J. Am. Chem. Soc. 2002, 124, 10254–10255. [PubMed: 12197708]

(31). Martí AA Metal Complexes and Time-Resolved Photoluminescence Spectroscopy for Sensing Applications. J. Photochem. Photobiol. Chem. 2015, 307–308, 35–47.

(32). Huang K; Jiang C; Martí AA Ascertaining Free Histidine from Mixtures with Histidine-Containing Proteins Using Time-Resolved Photoluminescence Spectroscopy. J. Phys. Chem. A 2014, 118, 10353–10358. [PubMed: 25313943]

(33). Sreedharan S; Sinopoli A; Jarman PJ; Robinson D; Clemmet C; Scattergood PA; Rice CR; Smythe CGW; Thomas JA; Elliott PIP Mitochondria-Localising DNA-Binding Biscyclometalated Phenyltriazole Iridium(III) Dipyridophenazene Complexes: Syntheses and Cellular Imaging Properties. Dalton Trans. 2018, 47, 4931–4940. [PubMed: 29552680]

(34). Liu H-W; Law WH-T; Lee LC-C; Lau JC-W; Lo KK-W Cyclometalated Iridium(III) Bipyridine-Phenylboronic Acid Complexes as Bioimaging Reagents and Luminescent Probes for Sialic Acids. Chem. - Asian J. 2017, 12, 1545–1556. [PubMed: 28418182]

(35). Wang W; Lu L; Wu K-J; Liu J; Leung C-H; Wong C-Y; Ma D-L Long-Lived Iridium(III) Complexes as Luminescent Probes for the Detection of Periodate in Living Cells. Sens. Actuators, B 2019, 288, 392–398.

(36). Zhang C; Qiu K; Liu C; Huang H; Rees TW; Ji L; Zhang Q; Chao H Tracking Mitochondrial Dynamics during Apoptosis with Phosphorescent Fluorinated Iridium(III) Complexes. Dalton Trans. 2018, 47, 12907–12913. [PubMed: 30117504]

(37). Wu X; Zheng Y; Wang F; Cao J; Zhang H; Zhang D; Tan C; Ji L; Mao Z Anticancer Ir III –Aspirin Conjugates for Enhanced Metabolic Immuno-Modulation and Mitochondrial Lifetime Imaging. Chem. - Eur. J. 2019, 25, 7012–7022. [PubMed: 30913329]

(38). Shaikh S; Wang Y; ur Rehman F; Jiang H; Wang X Phosphorescent Ir (III) Complexes as Cellular Staining Agents for Biomedical Molecular Imaging. Coord. Chem. Rev. 2020, 416, No. 213344.

(39). Wang W; Wu K; Vellaisamy K; Leung C; Ma D Peptide-Conjugated Long-Lived Theranostic Imaging for Targeting GRPr in Cancer and Immune Cells. Angew. Chem., Int. Ed. 2020, 59, 17897–17902.

(40). Zhu J; Tang BZ; Lo KK Luminescent Molecular Octopuses with a Polyhedral Oligomeric Silsesquioxane (POSS) Core and Iridium(III) Polypyridine Arms: Synthesis, Aggregation Induced Emission, Cellular Uptake, and Bioimaging Studies. Chem. - Eur. J. 2019, 25, 10633–10641. [PubMed: 31025784]

(41). Zhang P; Huang H; Banerjee S; Clarkson GJ; Ge C; Imberti C; Sadler PJ Nucleus-Targeted Organoiridium–Albumin Conjugate for Photodynamic Cancer Therapy. Angew. Chem., Int. Ed. 2019, 58, 2350–2354.

(42). Denison M; Steinke SJ; Majeed A; Turro C; Kocarek TA; Sevrioukova IF; Kodanko JJ Ir(III)-Based Agents for Monitoring the Cytochrome P450 3A4 Active Site Occupancy. Inorg. Chem. 2022, 61, 13673–13677. [PubMed: 35994607]

(43). Toupin N; Steinke SJ; Nadella S; Li A; Rohrabaugh TN; Samuels ER; Turro C; Sevrioukova IF; Kodanko JJ Photosensitive Ru(II) Complexes as Inhibitors of the Major Human Drug Metabolizing Enzyme CYP3A4. J. Am. Chem. Soc. 2021, 143, 9191–9205. [PubMed: 34110801]

(44). Zanoni KPS; Kariyazaki BK; Ito A; Brennaman MK; Meyer TJ; Murakami Iha NY Blue-Green Iridium(III) Emitter and Comprehensive Photophysical Elucidation of Heteroleptic Cyclometalated Iridium(III) Complexes. Inorg. Chem. 2014, 53, 4089–4099. [PubMed: 24684677]

(45). Yoshihara T; Murayama S; Masuda T; Kikuchi T; Yoshida K; Hosaka M; Tobita S Mitochondria-Targeted Oxygen Probes Based on Cationic Iridium Complexes with a 5-Amino-1, 10-Phenanthroline Ligand. J. Photochem. Photobiol. Chem. 2015, 299, 172–182.

(46). Li Y; Wu Y; Chen L; Zeng H; Chen X; Lun W; Fan X; Wong W-Y A Time-Resolved near-Infrared Phosphorescent Iridium-(III) Complex for Fast and Highly Specific Peroxynitrite Detection and Bioimaging Applications. J. Mater. Chem. B 2019, 7, 7612–7618. [PubMed: 31746928]

(47). Sevrioukova IF; Poulos TL Structure and Mechanism of the Complex between Cytochrome P4503A4 and Ritonavir. Proc. Natl. Acad. Sci. U.S.A. 2010, 107, 18422–18427. [PubMed: 20937904]

(48). Pavlovic D.; Mutak S.; Andreotti D.; Biondi S.; Cardullo F.; Paio A.; Piga E.; Donati D.; Lociuro S. Synthesis and Structure-Activity Relationships of α-Amino-γ-Lactone Ketolides: A Novel Class of Macrolide Antibiotics. ACS Med. Chem. Lett. 2014, 5, 1133–1137. [PubMed: 25313326]

(49). Chen Y; Liu C; Wang L Effects of Fluorine Substituent on Properties of Cyclometalated Iridium(III) Complexes with a 2,2′-Bipyridine Ancillary Ligand. Tetrahedron 2019, 75, No. 130686.

(50). Xiang H; Chen H; Tham HP; Phua SZF; Liu J-G; Zhao Y Cyclometalated Iridium(III)-Complex-Based Micelles for Glutathione-Responsive Targeted Chemotherapy and Photodynamic Therapy. ACS Appl. Mater. Interfaces 2017, 9, 27553–27562. [PubMed: 28749655]

(51). Kwon T-H; Oh YH; Shin I-S; Hong J-I New Approach Toward Fast Response Light-Emitting Electrochemical Cells Based on Neutral Iridium Complexes via Cation Transport. Adv. Funct. Mater. 2009, 19, 711–717.

(52). Dai Y; Zhan Z; Chai L; Zhang L; Guo Q; Zhang K; Lv Y A Two-Photon Excited Near-Infrared Iridium(III) Complex for Multi-Signal Detection and Multimodal Imaging of Hypochlorite. Anal. Chem. 2021, 93, 4628–4634. [PubMed: 33656847]

(53). Helms M; Lin Z; Gong L; Harms K; Meggers E Method for the Preparation of Nonracemic Bis-Cyclometalated Iridium(III) Complexes. Eur. J. Inorg. Chem. 2013, 2013, 4164–4172.

(54). Macé A; Hellou N; Hammoud J; Martin C; Gauthier ES; Favereau L; Roisnel T; Caytan E; Nasser G; Vanthuyne N; Williams JAG; Berrée F; Carboni B; Crassous J An Enantiopure

Cyclometallated Iridium Complex Displaying Long-Lived Phosphorescence Both in Solution and in the Solid State. Helv. Chim. Acta 2019, 102, No. e1900044.

(55). Manguin R; Pichon D; Tarrieu R; Vives T; Roisnel T; Dorcet V; Crévisy C; Miqueu K; Favereau L; Crassous J; Mauduit M; Baslé O A Kinetic Resolution Strategy for the Synthesis of Chiral Octahedral NHC–Iridium(iii) Catalysts. Chem. Commun. 2019, 55, 6058–6061.

(56). Li L-P; Yao S-Y; Ou Y-L; Wei L-Q; Ye B-H Diastereoselective Synthesis and Photophysical Properties of Bis-Cyclometalated Ir(III) Stereoisomers with Dual Stereocenters. Organometallics 2017, 36, 3257–3265.

(57). Yao S-Y; Ou Y-L; Ye B-H Asymmetric Synthesis of Enantiomerically Pure Mono- and Binuclear Bis(Cyclometalated) Iridium(III) Complexes. Inorg. Chem. 2016, 55, 6018–6026. [PubMed: 27280959]

(58). Cao M; Zhu J; Zhi Z; Ye B; Yao S; Zhang X Thermodynamic Resolution of Pharmaceutical Precursor Modafinil Acid on the Basis of Chiral-at-Metal Strategy. Chin. J. Chem. 2021, 39, 1483–1490.

(59). Mietke T; Cruchter T; Winterling E; Tripp M; Harms K; Meggers E Suzuki Cross-Coupling for Post-Complexation Derivatization of Non-Racemic Bis-Cyclometalated Iridium(III) Complexes. Chem. – Eur. J. 2017, 23, 12363–12371. [PubMed: 28560718]

(60). Cruchter T; Medvedev MG; Shen X; Mietke T; Harms K; Marsch M; Meggers E Asymmetric Nucleophilic Catalysis with an Octahedral Chiral-at-Metal Iridium(III) Complex. ACS Catal. 2017, 7, 5151–5162.

(61). Shen X; Huo H; Wang C; Zhang B; Harms K; Meggers E Octahedral Chiral-at-Metal Iridium Catalysts: Versatile Chiral Lewis Acids for Asymmetric Conjugate Additions. Chem. – Eur. J. 2015, 21, 9720–9726. [PubMed: 26033287]

(62). Xiong M-F; Peng H-L; Zhang X-P; Ye B-H Discrepancy between Proline and Homoproline in Chiral Recognition and Diastereomeric Photoreactivity with Iridium(III) Complexes. Inorg. Chem. 2021, 60, 5423–5431. [PubMed: 33818063]

(63). Li L-P; Peng H-L; Ye B-H Chiral Sensor for Enantiomeric Purity of Amines, Amino Alcohols and Amino Esters Based on Bis-Cyclometalated Ir(III) Complex Using 1H NMR Spectroscopy. Inorg. Chim. Acta 2018, 482, 691–697.

(64). Martir DR; Momblona C; Pertegás A; Cordes DB; Slawin AMZ; Bolink HJ; Zysman-Colman E Chiral Iridium(III) Complexes in Light-Emitting Electrochemical Cells: Exploring the Impact of Stereochemistry on the Photophysical Properties and Device Performances. ACS Appl. Mater. Interfaces 2016, 8, 33907–33915. [PubMed: 27960443]

(65). Kang T-S; Mao Z; Ng C-T; Wang M; Wang W; Wang C; Lee SM-Y; Wang Y; Leung C-H; Ma D-L Identification of an Iridium(III)-Based Inhibitor of Tumor Necrosis Factor-α. J. Med. Chem. 2016, 59, 4026–4031. [PubMed: 27054262]

(66). Whang DR; Sakai K; Park SY Highly Efficient Photocatalytic Water Reduction with Robust Iridium(III) Photosensitizers Containing Arylsilyl Substituents. Angew. Chem., Int. Ed. 2013, 52, 11612–11615.

(67). Alrawashdeh LR; Cronin MP; Woodward CE; Day AI; Wallace L Iridium Cyclometalated Complexes in Host–Guest Chemistry: A Strategy for Maximizing Quantum Yield in Aqueous Media. Inorg. Chem. 2016, 55, 6759–6769. [PubMed: 27315543]

(68). Nam JS; Kang M-G; Kang J; Park S-Y; Lee SJC; Kim H-T; Seo JK; Kwon O-H; Lim MH; Rhee H-W; Kwon T-H Endoplasmic Reticulum-Localized Iridium(III) Complexes as Efficient Photodynamic Therapy Agents via Protein Modifications. J. Am. Chem. Soc. 2016, 138, 10968–10977. [PubMed: 27494510]

(69). Flamigni L; Barbieri A; Sabatini C; Ventura B; Barigelletti F Photochemistry and Photophysics of Coordination Compounds: Iridium. In Photochemistry and Photophysics of Coordination Compounds II; Balzani V., Campagna S., Eds.; Springer Berlin Heidelberg: Berlin, Heidelberg, 2007; pp 143–203.

(70). Gao R; Ho DG; Hernandez B; Selke M; Murphy D; Djurovich PI; Thompson ME Bis-Cyclometalated Ir(III) Complexes as Efficient Singlet Oxygen Sensitizers. J. Am. Chem. Soc. 2002, 124, 14828–14829. [PubMed: 12475307]

(71). Goldstein BM; Barton JK; Berman HM Crystal and Molecular Structure of a Chiral-Specific DNA-Binding Agent: Tris(4,7-Diphenyl-1,10-Phenanthroline)Ruthenium(II). Inorg. Chem. 1986, 25, 842–847.

(72). Pyle AM; Morii T; Barton JK Probing Microstructures in Double-Helical DNA with Chiral Metal Complexes: Recognition of Changes in Base-Pair Propeller Twisting in Solution. J. Am. Chem. Soc. 1990, 112, 9432–9434.

(73). Maksimoska J; Feng L; Harms K; Yi C; Kissil J; Marmorstein R; Meggers E Targeting Large Kinase Active Site with Rigid, Bulky Octahedral Ruthenium Complexes. J. Am. Chem. Soc. 2008, 130, 15764–15765. [PubMed: 18973295]

(74). Göbel P; Ritterbusch F; Helms M; Bischof M; Harms K; Jung M; Meggers E Probing Chiral Recognition of Enzyme Active Sites with Octahedral Iridium(III) Propeller Complexes. Eur. J. Inorg. Chem. 2015, 2015, 1654–1659.

(75). Chen S; Wu Q; Li X; Li D; Mei N; Ning B; Puig M; Ren Z; Tolleson WH; Guo L Characterization of Cytochrome P450s (CYP)-Overexpressing HepG2 Cells for Assessing Drug and Chemical-Induced Liver Toxicity. J. Environ. Sci. Health, Part C: Toxicol. Carcinog. 2021, 39, 68–86.

(76). Xuan J; Chen S; Ning B; Tolleson WH; Guo L Development of HepG2-Derived Cells Expressing Cytochrome P450s for Assessing Metabolism-Associated Drug-Induced Liver Toxicity. Chem. Biol. Interact. 2016, 255, 63–73. [PubMed: 26477383]

(77). Yoshitomi S; Ikemoto K; Takahashi J; Miki H; Namba M; Asahi S Establishment of the Transformants Expressing Human Cytochrome P450 Subtypes in HepG2, and Their Applications on Drug Metabolism and Toxicology. Toxicol. In Vitro 2001, 15, 245–256. [PubMed: 11377097]

(78). Samuels ER; Sevrioukova I Structure–Activity Relationships of Rationally Designed Ritonavir Analogues: Impact of Side-Group Stereochemistry, Headgroup Spacing, and Backbone Composition on the Interaction with CYP3A4. Biochemistry 2019, 58, 2077–2087. [PubMed: 30912932]

(79). Kumar GN; Rodrigues AD; Buko AM; Denissen JF CytochromeP450-Mediated Metabolismof the HIV-1 Protease InhibitorRitonavir(ABT-538)in HumanLiverMicrosomes. J. Pharmacol. Exp. Ther. 1996, 277, 423–431. [PubMed: 8613951]

(80). Sevrioukova IF; Poulos TL Structural Basis for Regiospecific Midazolam Oxidation by Human Cytochrome P450 3A4. Proc. Natl. Acad. Sci. U.S.A. 2017, 114, 486–491. [PubMed: 28031486]

(81). Mak PJ; Denisov IG Spectroscopic Studies of the Cytochrome P450 Reaction Mechanisms. Biochim. Biophys. Acta, Proteins Proteomics 2019, 1866, 178–204.

(82). Anthony EJ; Bolitho EM; Bridgewater HE; Carter OWL; Donnelly JM; Imberti C; Lant EC; Lermyte F; Needham RJ; Palau M; Sadler PJ; Shi H; Wang F-X; Zhang W-Y; Zhang Z Metallodrugs Are Unique: Opportunities and Challenges of Discovery and Development. Chem. Sci. 2020, 11, 12888–12917. [PubMed: 34123239]

(83). Meggers E Targeting Proteins with Metal Complexes. Chem. Commun. 2009, 9, 1001.

(84). Hartinger CG; Metzler-Nolte N; Dyson PJ Challenges and Opportunities in the Development of Organometallic Anticancer Drugs. Organometallics 2012, 31, 5677–5685.

(85). Wu S; Zhou Y; Rebelein JG; Kuhn M; Mallin H; Zhao J; Igareta NV; Ward TR Breaking Symmetry: Engineering Single-Chain Dimeric Streptavidin as Host for Artificial Metalloenzymes. J. Am. Chem. Soc. 2019, 141, 15869–15878. [PubMed: 31509711]

(86). Feng L; Geisselbrecht Y; Blanck S; Wilbuer A; Atilla-Gokcumen GE; Filippakopoulos P; Kräling K; Celik MA; Harms K; Maksimoska J; Marmorstein R; Frenking G; Knapp S; Essen L-O; Meggers E Structurally Sophisticated Octahedral Metal Complexes as Highly Selective Protein Kinase Inhibitors. J. Am. Chem. Soc. 2011, 133, 5976–5986. [PubMed: 21446733]

(87). Rebelein JG; Cotelle Y; Garabedian B; Ward TR Chemical Optimization of Whole-Cell Transfer Hydrogenation Using Carbonic Anhydrase as Host Protein. ACS Catal. 2019, 9, 4173–4178. [PubMed: 31080690]

(88). Monnard FW; Nogueira ES; Heinisch T; Schirmer T; Ward TR Human Carbonic Anhydrase II as Host Protein for the Creation of Artificial Metalloenzymes: The Asymmetric Transfer Hydrogenation of Imines. Chem. Sci. 2013, 4, 3269.

(89). Sullivan MP; Cziferszky M; Tolbatov I; Truong D; Mercadante D; Re N; Gust R; Goldstone DC; Hartinger CG Probing the Paradigm of Promiscuity for N-Heterocyclic Carbene Complexes and Their Protein Adduct Formation. Angew. Chem., Int. Ed. 2021, 60, 19928–19932.

(90). Robles VM; Dürrenberger M.; Heinisch T.; Lledós A.; Schirmer T.; Ward TR.; Maréchal J-D. Structural, Kinetic, and Docking Studies of Artificial Imine Reductases Based on Biotin–Streptavidin Technology: An Induced Lock-and-Key Hypothesis. J. Am. Chem. Soc. 2014, 136, 15676–15683. [PubMed: 25317660]

(91). Heinisch T; Pellizzoni M; Dürrenberger M.; Tinberg CE.; Köhler V.; Klehr J.; Häussinger D.; Baker D.; Ward TR. Improving the Catalytic Performance of an Artificial Metalloenzyme by Computational Design. J. Am. Chem. Soc. 2015, 137, 10414–10419. [PubMed: 26226626]

(92). Stein A; Chen D; Igareta NV; Cotelle Y; Rebelein JG; Ward TR A Dual Anchoring Strategy for the Directed Evolution of Improved Artificial Transfer Hydrogenases Based on Carbonic Anhydrase. ACS Cent. Sci. 2021, 7, 1874–1884. [PubMed: 34849402]

(93). Koren K; Dmitriev RI; Borisov SM; Papkovsky DB; Klimant I Complexes of Ir(III)-Octaethylporphyrin with Peptides as Probes for Sensing Cellular O2. ChemBioChem 2012, 13, 1184–1190. [PubMed: 22532338]

(94). Zhang KY; Zhang T; Wei H; Wu Q; Liu S; Zhao Q; Huang W Phosphorescent Iridium(iii) Complexes Capable of Imaging and Distinguishing between Exogenous and Endogenous Analytes in Living Cells. Chem. Sci. 2018, 9, 7236–7240. [PubMed: 30288243]

(95). Zhang KY; Gao P; Sun G; Zhang T; Li X; Liu S; Zhao Q; Lo KK-W; Huang W Dual-Phosphorescent Iridium(III) Complexes Extending Oxygen Sensing from Hypoxia to Hyperoxia. J. Am. Chem. Soc. 2018, 140, 7827–7834. [PubMed: 29874455]

(96). Li SP-Y; Shum J; Lo KK-W Iridium(iii) Polypyridine Complexes with a Disulfide Linker as Biological Sensors and Cytotoxic Agents. Dalton Trans. 2019, 48, 9692–9702. [PubMed: 30949652]

(97). Xiong L; Zhao Q; Chen H; Wu Y; Dong Z; Zhou Z; Li F Phosphorescence Imaging of Homocysteine and Cysteine in Living Cells Based on a Cationic Iridium(III) Complex. Inorg. Chem. 2010, 49, 6402–6408. [PubMed: 20565069]

(98). Wang X; Zhang J; Zhao X; Wei W; Zhao J Imaging and Proteomic Study of a Clickable Iridium Complex. Metallomics 2019, 11, 1344–1352. [PubMed: 31347624]

(99). Leung PK-K; Lee LC-C; Yeung HH-Y; Io K-W; Lo KK-W Bioorthogonal Control of the Phosphorescence and Singlet Oxygen Photosensitisation Properties of Iridium(iii) Tetrazine Complexes. Chem. Commun. 2021, 57, 4914–4917.

(100). Teo YL; Ho HK; Chan A Metabolism-Related Pharmacokinetic Drug-Drug Interactions with Tyrosine Kinase Inhibitors: Current Understanding, Challenges and Recommendations. Br. J. Clin. Pharmacol. 2015, 79, 241–253. [PubMed: 25125025]

(101). Thummel KE; Wilkinson GR In Vitro and In Vivo Drug Interactions Involving Human CYP3A. Annu. Rev. Pharmacol. Toxicol. 1998, 38, 389–430. [PubMed: 9597161]

(102). van Eijk M; Boosman RJ; Schinkel AH; Huitema ADR; Beijnen JH Cytochrome P450 3A4, 3A5, and 2C8 Expression in Breast, Prostate, Lung, Endometrial, and Ovarian Tumors: Relevance for Resistance to Taxanes. Cancer Chemother. Pharmacol. 2019, 84, 487–499. [PubMed: 31309254]

(103). Breslin S; Lowry MC; O'Driscoll L Neratinib Resistance and Cross-Resistance to Other HER2-Targeted Drugs Due to Increased Activity of Metabolism Enzyme Cytochrome P4503A4. Br. J. Cancer 2017, 116, 620–625. [PubMed: 28152547]

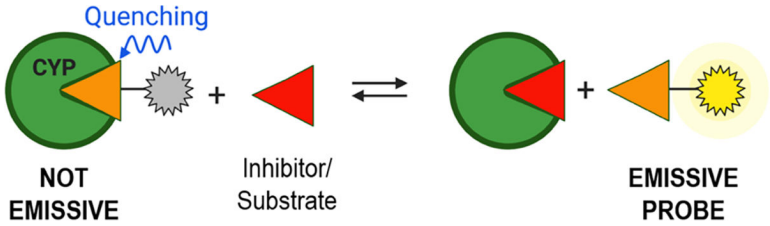

Figure 1.

Emission quenching of Ir(III) by CYP3A4 followed by reversible emission turn in the presence of CYP3A4 inhibitor or substrate.

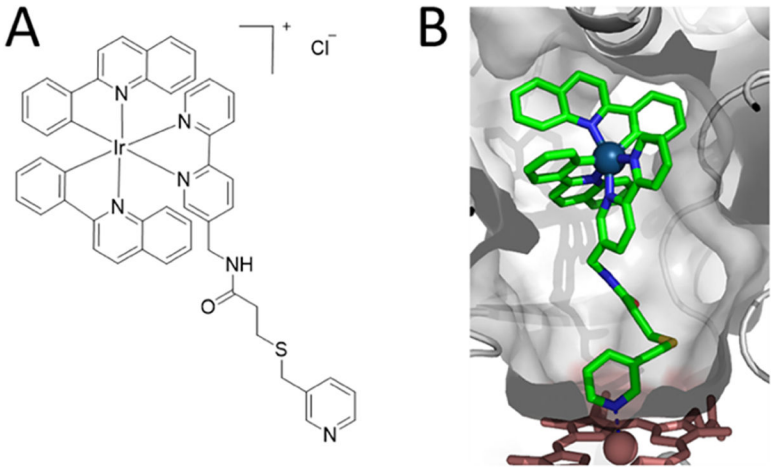

Figure 2.
Chemical structure (A) and crystal structure (B) of the previously reported Ir(III)-based probe bound to the active site of CYP3A4 (2.78 Å; PDB ID 7UAY).

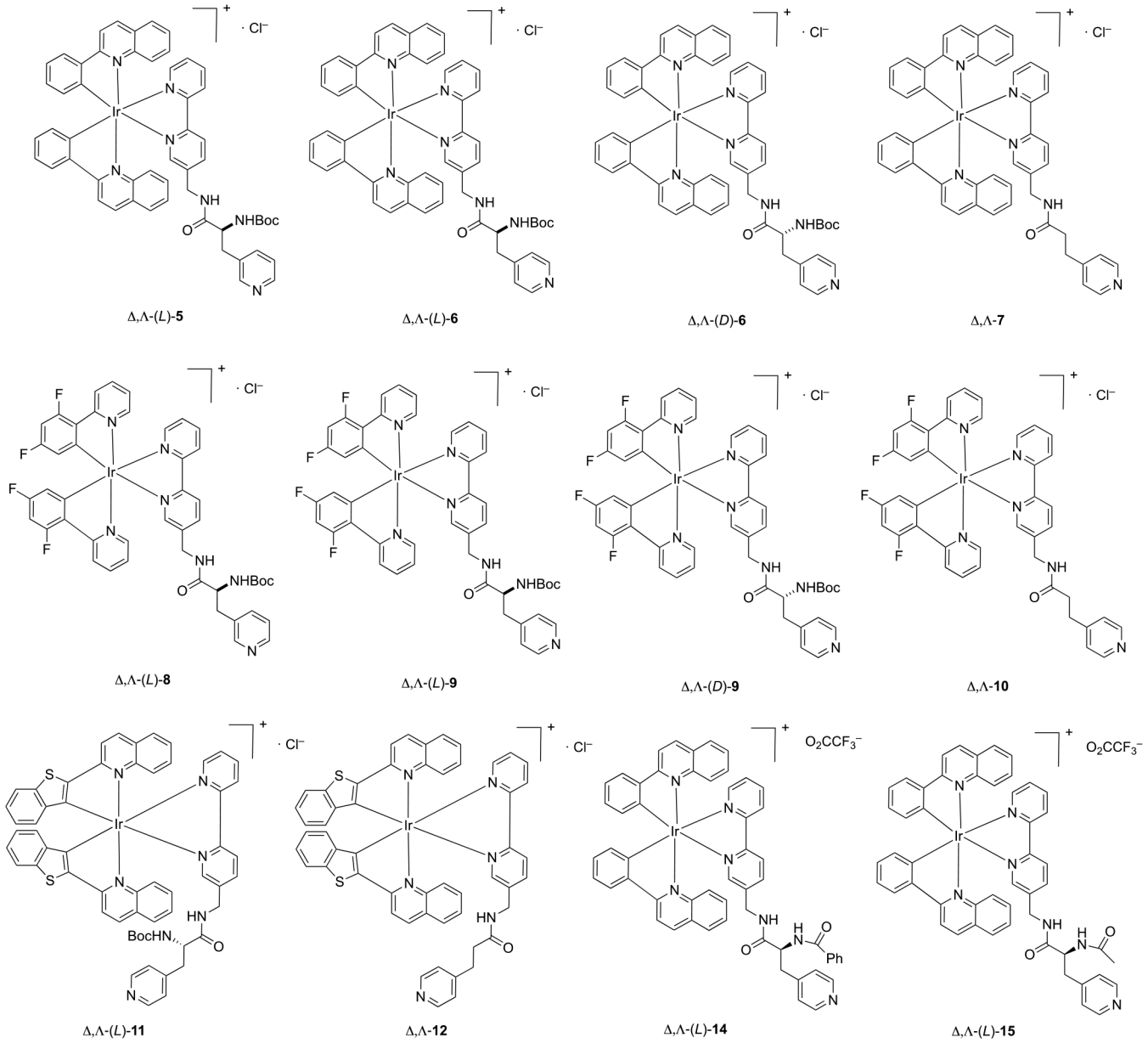

Figure 3.
Structures of compounds 1−15 (Δ,Λ-Ir(III) complexes).

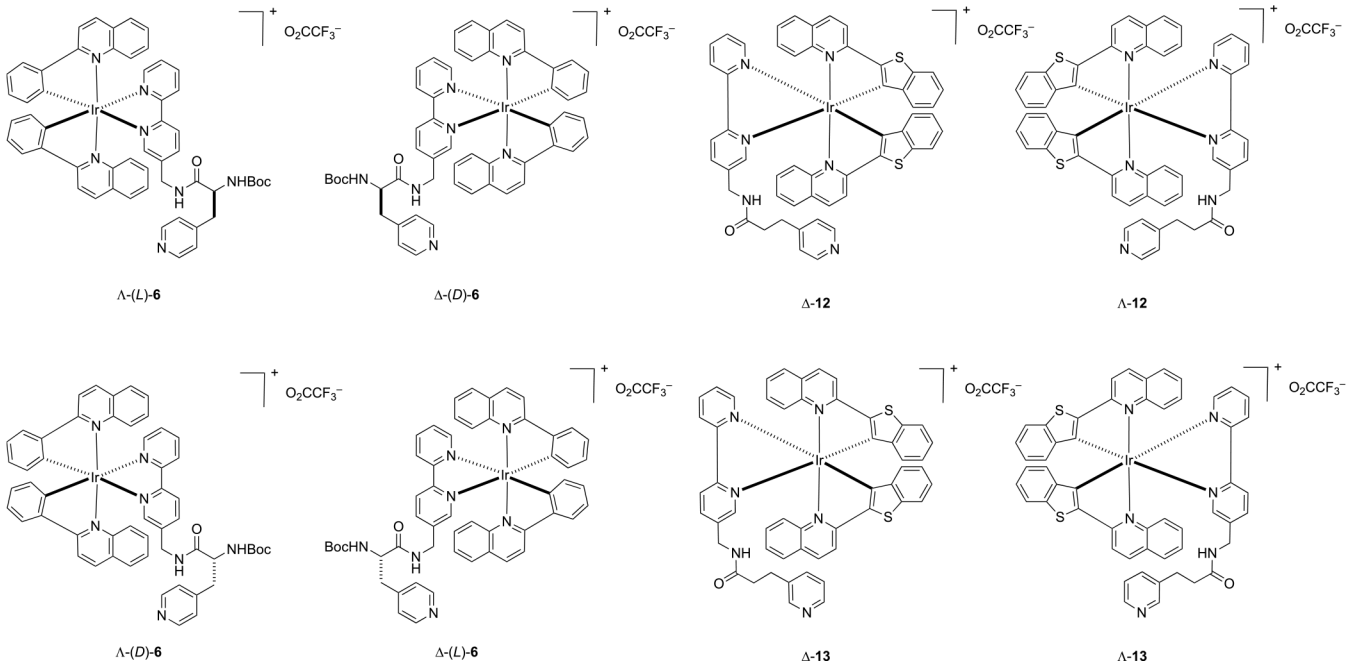

Figure 4.
Structures of resolved stereoisomers **6**, **12**, and **13**.

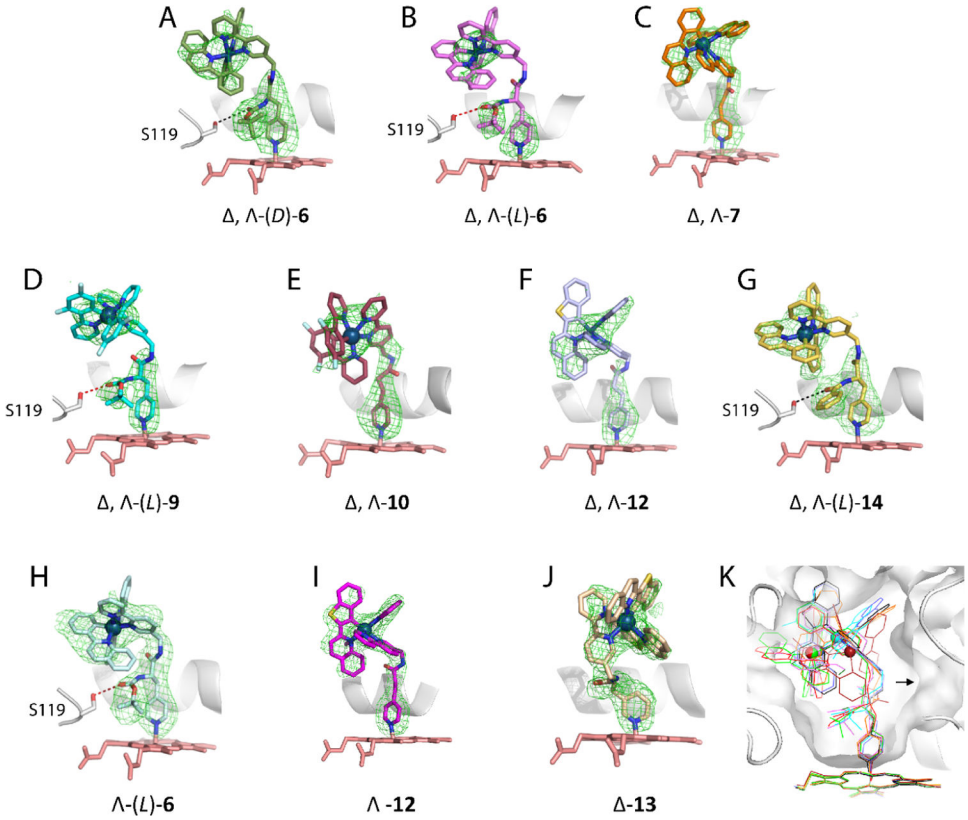

Figure 5.

Crystal structures of CYP3A4 bound to the inhibitory compounds from the new series of Ir(III) probes. Racemic (L)-6, (D)-6, 7, (L)-9, 10, 12, and (L)-14 (A–G, respectively) and stereoisomers Λ-(L)-6, Λ-12, and Δ-13 (H–J, respectively) bind to the active site and ligate to the heme via the end-pyridine moiety. All probes are similarly oriented relative to the central I-helix. Δ,Λ-(L)-6, Δ,Λ-9, and Λ-(L)-6 form hydrogen bonds with Ser119 (red dotted lines). The side groups of Δ,Λ-(D)-6 and Δ,Λ-(L)-14 are too far for H-bond formation but can establish long-distance polar interactions with Ser119 (black dotted lines). Polder omit electron density maps contoured at 3σ level are shown as green mesh. (K) Structural overlay of all compounds except the *meta*-pyridine containing Δ-13. The Ir atoms are shown as spheres to demonstrate the distinct cage positioning. A large pocket above the I-helix, which can be filled to improve the inhibitory potency, is indicated by an arrow.

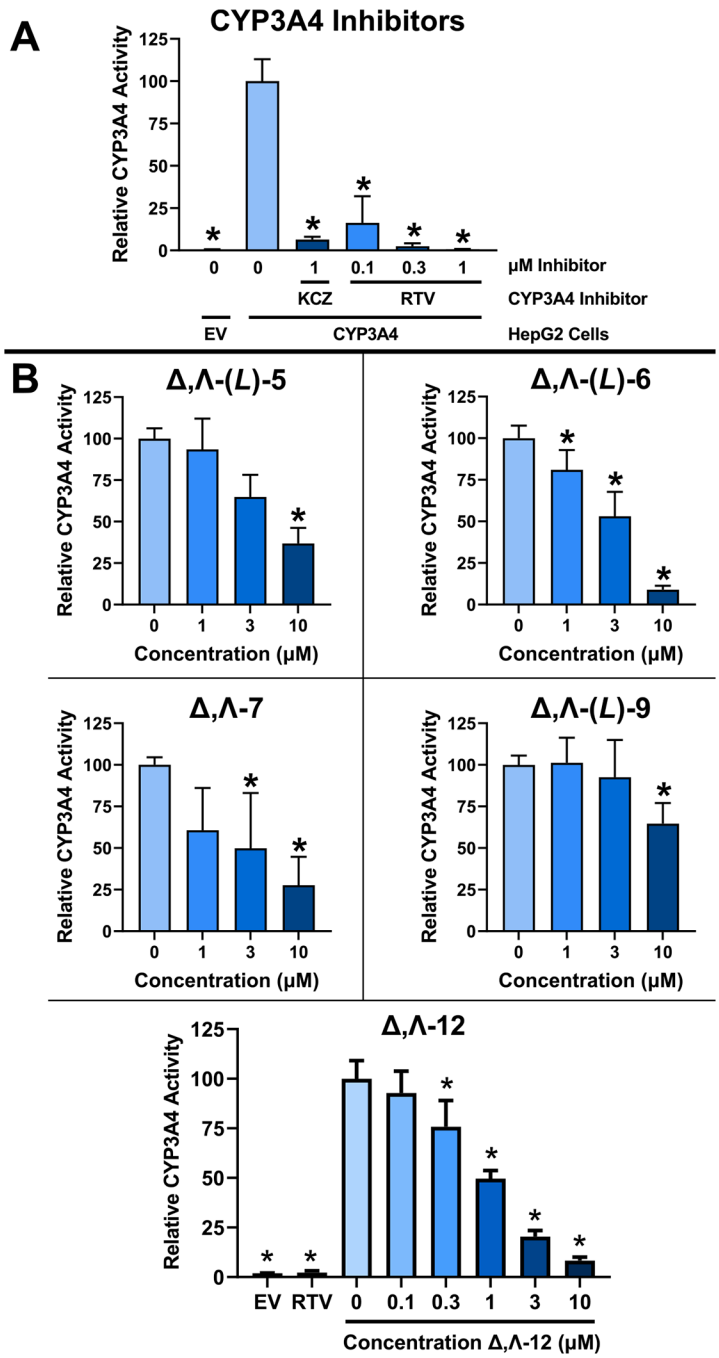

Figure 6.

Inhibition of CYP3A4 activity by Ir(III) compounds in HepG2-CYP3A4 cells. (A) Effects of known potent inhibitors of CYP3A4, used as positive controls, on CYP3A4 activity in HepG2-CYP3A4 cells. HepG2-CYP3A4 cells were incubated with 1 μM ketoconazole (KCZ) or 0.1, 0.3, or 1 μM ritonavir (RTV) and CYP3A4 activity was measured using the P450-Glo CYP3A4 Assay, as described in the Materials and Methods section. The negligible CYP3A4 activity in HepG2-EV cells is shown for comparison. (B) HepG2-CYP3A4 cells were incubated with the indicated concentrations of racemic compound (L)-**5**, (L)-**6**, **7**, (L)-**9**,

or **12** before CYP3A4 activity was measured. Data are shown as mean percent CYP3A4 activity relative to a control group (HepG2-CYP3A4 cells incubated with 0.1% DMSO [0 μM inhibitor]) ± SD (n = 9 or 12; from three or four experiments, three replicates per experiment). *Significantly different from the control group by one-way analysis of variance and Dunnett's multiple comparison test, $P < 0.05$.

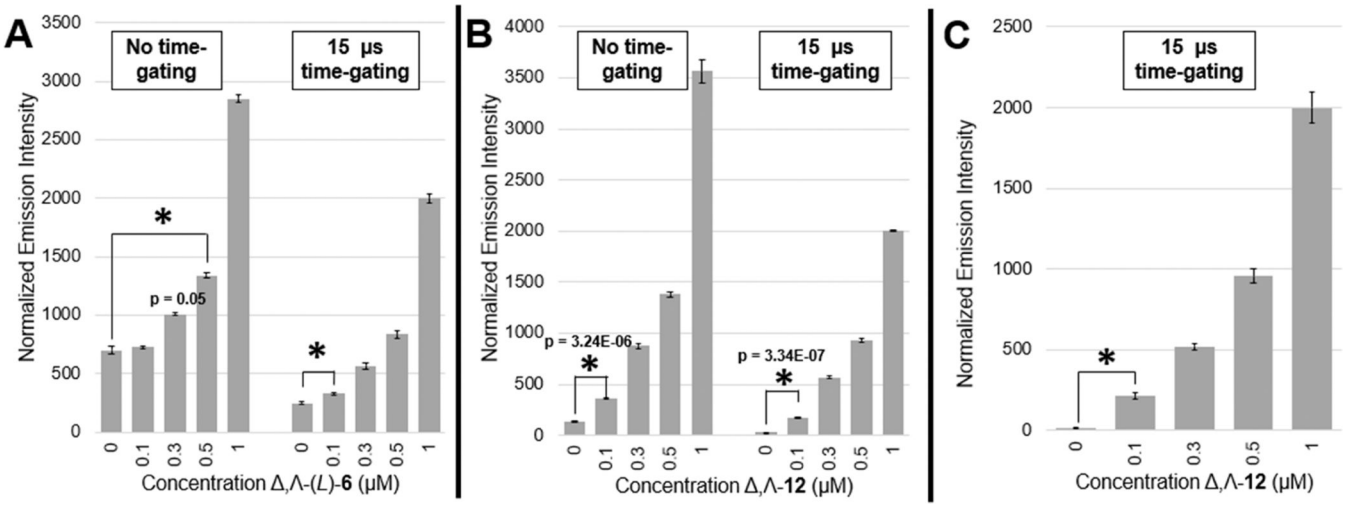

Figure 7.

Normalized emission intensity of Δ,Λ-(L)-**6** and Δ,Λ-**12** in Williams' Media E without (A, B) or with HepG2-CYP3A4 cells (C). Media contains 10% FBS, 1% glutamine, and 1000 U/mL penicillin/streptomycin. Data are the average of quadruplicate wells; errors are shown as standard deviations. (A) Bar graph showing differences in emission intensity as a function of concentration of Δ,Λ-(L)-6 with 0 and 15 μs time-gating. Statistical significance (*$p \leq 0.05$) is found at 500 nM ($p = 0.05$ at 300 nM) without time-gating and at 100 nM with 15 μs time-gating. (B) Bar graph showing differences in emission intensity as a function of concentration of Δ,Λ-**12** with 0 and 15 μs time-gating. Statistical significance is found at 100 nM with and without time-gating. (C) Bar graph showing differences in emission intensity as a function of concentration of Δ,Λ-**12** with 15 μs time-gating in HepG2-CYP3A4 cells. Cells were seeded in 96-well plates (7000 cells/well) and incubated for 18 h before treatment with compounds (100 nM to 1 μM) or vehicle control. Treated cells were incubated for 4 h before emission measurements were taken.

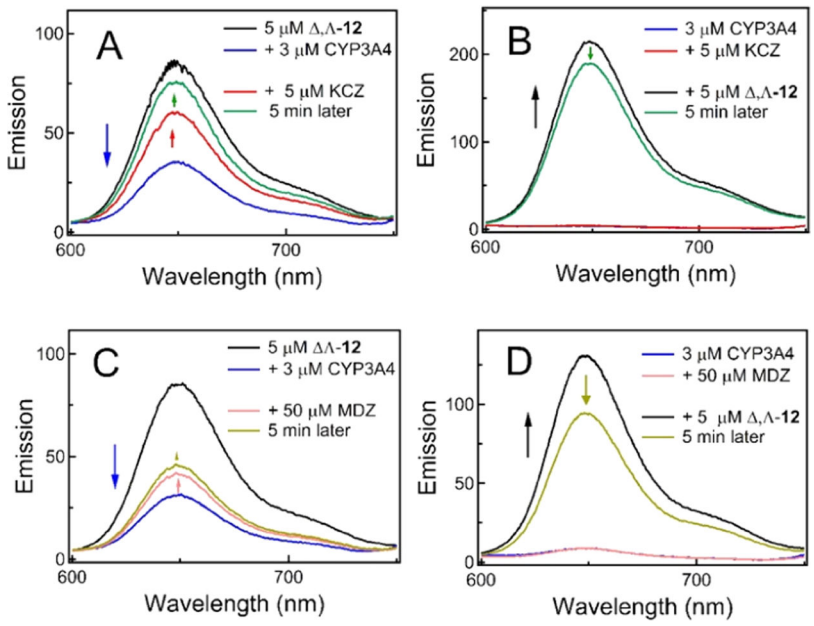

Figure 8.

Fluorescent changes observed during competitive ligand binding to CYP3A4. Fluorescence changes in 5 μM Δ,Λ-**12** were monitored in mixtures containing 3 μM CYP3A4 and 5 μM ketoconazole (KCZ) (A, B) or 50 μM midazolam (MDZ) (C, D), with λ_{ex} = 500 nm. Δ,Λ-**12** was added to CYP3A4 either before (A, C) or after the test compound (B, D). Arrows indicate direction of emission changes.

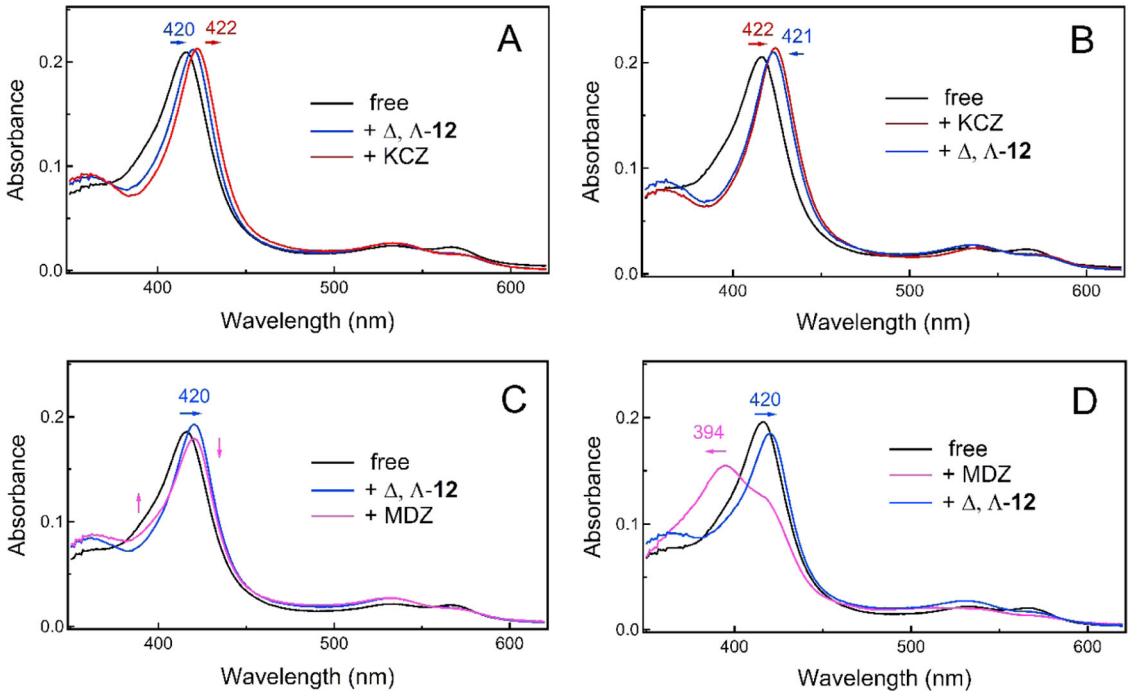

Figure 9.

Absorbance changes observed during competitive ligand binding to CYP3A4. Absorbance spectra of CYP3A4 (2 μM) were recorded in the absence and presence of Δ,Λ-**12** (3 μM) and the test inhibitor KCZ (3 μM) (A, B) or marker substrate MDZ (30 μM) (C, D). Δ,Λ-**12** was added to CYP3A4 either before (A, C) or after the test compound (B, D). Arrows indicate direction of absorbance changes.

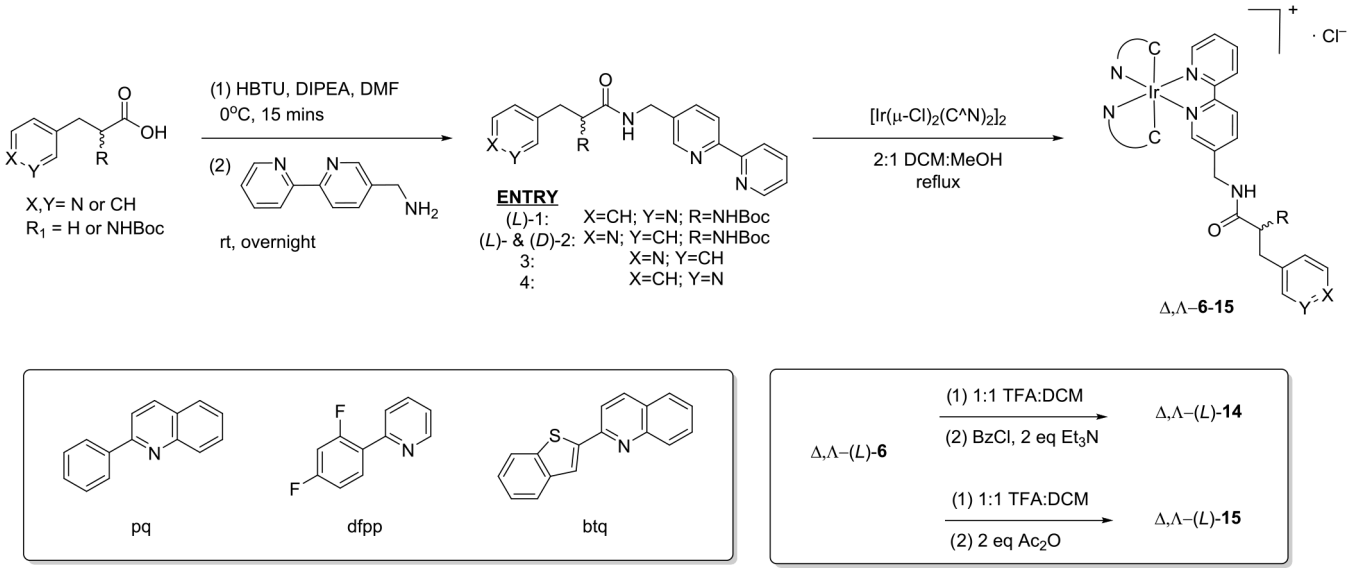

Scheme 1.

Synthesis of Compounds 1–15 (Δ,Λ-Ir(III) Complexes)[a]

[a]See Figure 3 for structures of Δ,Λ-6–15.

Table 1.

Δ,Λ-Ir(III) Complexes (5–15)

entry[a]	CΛN	X	Y	R_1
(L)-**5**	pq	CH	N	NHBoc
(L)- and (D) -**6**	pq	N	CH	NHBoc
7	pq	N	CH	H
(L)-**8**	dfpp	CH	N	NHBoc
(L)- and (D)-**9**	dfpp	N	CH	NHBoc
10	dfpp	N	CH	H
(L)-**11**	btq	N	CH	NHBoc
12	btq	N	CH	H
13 [b]	btq	CH	N	H
(L)-**14**	pq	N	CH	NHBz
(L)-**15**	pq	N	CH	NHAc

[a] Stereochemistry at the metal center is not specified here. Complexes were isolated as a mixture of **Δ,Λ** diastereomers with exception of **13.**

[b] **13** was not isolated as a mixture of diastereomers. **Δ-** and **Λ-13** were isolated separately as shown in Figure 4.

Table 2.

Lowest-Energy Absorption Maxima, λ_{max}, Emission Maxima, λ_{em}, Quantum Yields, Φ_{em}, and Lifetimes under Argon, τ_o, and Air, τ, of Complexes ΔΛ-5–15 in CH_3OH

complex[a]	λ_{max}/nm (ε/M $^{-1}$ cm^{-1})	λ_{em}/nm	Φ_{em}[b]	$\tau_o/\mu s$[c]	$\tau/\mu s$[c]
Δ,Λ-(L)-**5**	440 (7300)	560	0.18(2)	3.5	0.91
Δ,Λ-(L)-**6**	440 (6400)	559	0.167(6)	5.7	0.45
Δ,Λ-**7**	440 (5800)	558	0.10(2)	2.7	0.76
Δ,Λ-(L)-**8**	360 (7300)	528	0.16(4)	1.9	0.57
Δ,Λ-(L)-**9**	360 (7700)	530	0.135(1)	2.5	0.58
Δ,Λ-**10**	360 (6900)	527	0.14(3)	2.4	0.57
Δ,Λ-(L)-**11**	500 (10,000)	654	0.064(4)	6.8	0.67
Δ,Λ-**12**	500 (10,000)	653	0.072(1)	7.6	1.2
Δ,Λ-(L)-**14**	440 (6700)	556	0.17(7)	2.8	0.85
Δ,Λ-(L)-**15**	440 (5900)	559	0.16(2)	3.2	0.60

[a] Only racemic (**Δ,Λ**) complexes and L-stereoisomers (where stereochemistry is indicated) were analyzed.

[b] In deaerated H_2O with 5% CH_3OH to solubilize complexes, λ_{exc} = 440 nm for **5—7, 14,** and **15**; λ_{exc} = 360 nm for **8—10;** λ_{ex} = 500 nm for **11** and **12**.

[c] λ_{exc} = 355 nm, 5 mJ/pulse.

Table 3.

Emission Quantum Yields, Φ_{em}, and Lifetimes, τ, of Complexes Δ,Λ-7 and Δ,Λ-12 in CH_3OH, H_2O, and Cell Media in Air and under Argon

	Φ_Δ[a]	Φ_{em}[a]	τ/μs (MeOH, RT)[b]		τ/μs (H_2O, RT)[b]		τ/μ(cell media, 37 °C)[b]	
complex	**CH_3OH (air)**	**H_2O (argon)**	**argon**	**air**	**argon**	**air**	**argon**	**air**
Δ,Λ-7	1.1(2)	0.10(2)	2.7	0.76	1.7	0.70	1.8	1.0
Δ,Λ-12	1.1(2)	0.072(1)	7.6	1.2	3.9	2.2	5.3	3.8

[a] Quantum yields obtained in triplicate and referenced to $[Ru(bpy)_3]Cl_2$.

[b] λ_{exc} = 355 nm (5 mJ/pulse), monitored at the emission maximum.

Table 4.

Binding Affinity and Inhibitory Potency of Complexes 5—15 for CYP3A4

compound	K_d[a] (nM)	IC_{50}[b] (nM)
Δ,Λ-(L)-**5**	40 ± 2	171 ± 3
Δ,Λ-(L)-**6**	21 ± 6	134 ± 6
Δ-(L)-**6**	10 ± 1	143 ± 3
Λ-(L)-**6**	22 ± 5	120 ± 8
Δ,Λ-(D)-**6**	28 ± 6	124 ± 14
Δ-(D)-**6**	30 ± 4	140 ± 3
Λ-(D)-**6**	9 ±1	125 ± 4
Δ,Λ-**7**	133 ± 5	124 ± 4
Δ,Λ-(L)-**8**	35 ± 3	360 ± 35
Δ,Λ-(L)-**9**	13 ± 2	280 ± 20
Δ,Λ-(D)-**9**	43 ± 2	402 ± 16
Δ,Λ-**10**	356 ± 44	140 ± 17
Δ,Λ-(L)-**11**	40 ± 11	223 ± 17
Δ,Λ-**12**	24 ± 1	177 ± 3
Δ-**12**	15 ± 3	235 ± 5
Λ-**12**	52 ± 1	255 ± 4
Δ-**13**	29 ± 3	173 ± 12
Λ-**13**	30 ± 2	168 ± 25
Δ,Λ-(L)-**14**	26 ± 5	157 ± 2
Δ,Λ-(L)-**15**	46 ± 6	340 ± 22

Determined by spectrophotometric titration assay. Values represent an average of three independent measurements ± SD.

[b] CYP3A4 activity assay with BFC, 293 ± 3 K, 0.2 μM CYP3A4, 0.3 μM cytochrome P450 reductase, versus DMSO control (100% activity). Values represent an average of two duplicate measurements ± SD.

Table 5.

IC_{50} Values (μM) for Δ,Λ-(L)-6 and Δ,Λ-12 against Microsomal CYP3A4, CYP1A2, and CYP2C9[a]

	IC_{50} values (μM)			selectivity	
complex	**CYP3A4**	**CYP1A2**	**CYP2C9**	**CYP1A2:CYP3A4**	**CYP2C9:CYP3A4**
Δ,Λ-(L)-6	0.91 ± 0.07	>100	>100	>100	>100
Δ,Λ-12	2.3 ± 0.4	72 ± 5	17 ± 4	31	7.2

[a] IC_{50} values for Δ,Λ-(L)-**6** and Δ,Λ-**12** against CYP3A4, CYP1A2, and CYP2C9 were determined using commercially available inhibitor screening kits (BioVision) by following manufacturer's protocols. Stock Solutions of compounds were prepared in MeOH due to insolubility in MeCN.

Table 6.

EC_{50} Values (μM) for Complexes (L)-6, 7, (L)-8, and 12 in HepG2-CYP3A4 Cells[a]

complex	EC_{50}
Δ,Λ-(L)-6	21 ± 3
Δ,Λ-7	16 ± 3
Δ, Λ-(L)-8	>50
Δ, Λ-12	16 ± 5

[a] EC_{50} values (μM) for complexes (L)-**6**, **7**, (L)-**8**, and **12** were determined in HepG2-CYP3A4 cells. Data are the average of three independent experiments using quadruplicate wells; errors are shown as standard deviations. After treatment, the cells were incubated at 37 °C and 5% CO_2 for 72 h. Viability was then assessed by MTT assay, and EC_{50} values were obtained using Igor Pro graphing software.